Balancing Multiphase FCML Converters with Coupled Inductors: Modeling, Analysis, Limitations

Daniel H. Zhou, Student Member, IEEE, Janko Čeliković, Member, IEEE, Dragan Maksimović, Fellow, IEEE, and Minjie Chen, Senior Member, IEEE

Abstract—This paper investigates the modeling, analysis, and design methods for passively balancing flying capacitor multilevel (FCML) converters using coupled inductors. Coupled inductors synergize with FCML converters by reducing inductor current ripple, reducing switch stress, and, as proven in this paper, by providing flying capacitor voltage balancing. This enables FCML topologies to be scaled well to larger systems. This paper proves that coupled inductors can solve the unbalancing problem in many FCML converters. Moreover, tools are developed to thoroughly explain and quantify coupled inductor balancing. allowing general design guidelines to be offered for robust coupled inductor FCML converters. Finally, this paper derives the limitations of coupled inductor balancing with respect to the number of phases, levels, and the required coupling ratio. The key principles of coupled inductor FCML balancing in steadystate are demonstrated with a systematic theoretical framework and extensive experimental and simulation results.

Index Terms—flying capacitor multilevel (FCML) converter, coupled inductors, natural balancing, charge balancing, passive voltage balancing, feedback mechanism

I. INTRODUCTION

ultilevel converters are an important enabling technology for power converter applications requiring low current ripple and fast transient response, such as CPU voltage regulators [4], [5], envelope trackers, and power amplifiers [6], [7]. By using three or more switching voltage levels, multilevel converters can reduce the voltage and current stress on components and multiply the effective switching frequency. One method of generating more than the two switching voltage levels from a single input voltage is to use capacitors with dc voltages connected in series with the input supply. This is the working principle of flying capacitor multilevel (FCML) converters [8], which have proved especially effective in high bandwidth and high power converter designs [9]–[17].

Multilevel converters help to address one of the fundamental challenges of high bandwidth power converter designs: the

This paper is a combination and extension of three previously published conference papers at the 2021 IEEE Workshop on Control and Modeling for Power Electronics (COMPEL) [1], 2022 IEEE Applied Power Electronics Conference (APEC) [2], and 2022 IEEE Workshop on Control and Modeling for Power Electronics (COMPEL) [3].

Daniel H. Zhou and Minjie Chen are with the Department of Electrical Engineering and Andlinger Center for Energy and the Environment at Princeton University, Princeton, NJ, 08540, USA.

Janko Čeliković and Dragan Maksimovic are with the Department of Electrical, Computer and Energy Engineering and the Colorado Power Electronics Center at the University of Colorado, Boulder, CO, 80309, USA.

This work was supported in part by NSF CAREER Award No. 1847365, and in part by the NSERC PGS-D Award No. 557270-2021. We thank Kurtland Chua (Princeton University) for his assistance with mathematical derivations.

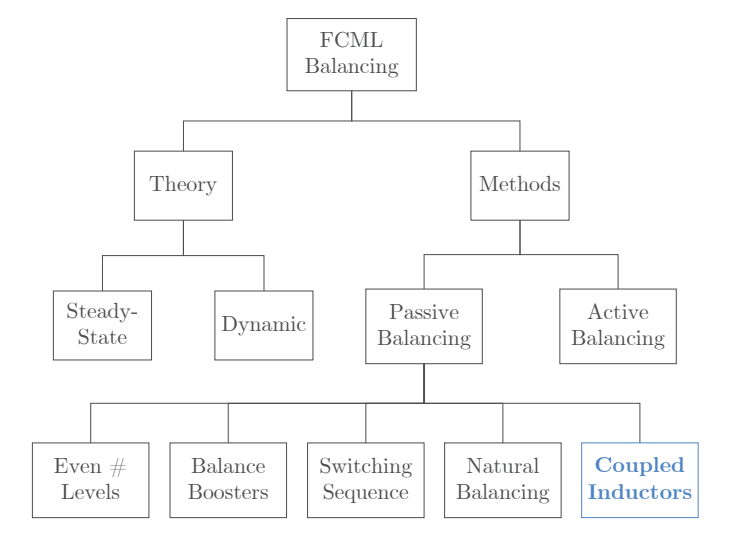


Fig. 1. Chart of selected research areas in FCML converter balancing. Coupled inductors represent a new branch of techniques for passively balancing FCML converters which can be used together with other techniques. Some of the highlighted balancing methods are compared in Section VII.

trade-off between current ripple and bandwidth presented by the inductive elements [4], [7], [18]. It is desirable to have a larger inductance to maintain low inductor current ripple, but it is also desirable to have a smaller inductance to respond to sudden load, input line, or output reference transients [15], [16], [19]. For a buck converter, the inductor selection must trade-off these two competing criteria. By switching between voltage levels that are closer together at a higher effective switching frequency, multilevel converters enable the use of smaller inductors without increasing the current ripple, thus circumventing the typical inductor trade-off.

FCML converters also synergize well with multiphase coupled inductors. Interleaving multiple converter phases with coupled inductors can reduce the inductor size [20], output current ripple [21], and transient inductance [22], [23]. Since coupled inductors reduce not only the overall current ripple but also that of the individual phases [24], [25], they can also reduce the core loss and saturation flux requirements. Finally, as proven in this paper, interleaving multiple FCML converters with coupled inductors passively balances the flying capacitors, overcoming the key limitation of FCML converters.

A. Background on FCML Converter Balancing

Despite their numerous advantages in theory, FCML converters only function well if the flying capacitors stay at

their ideally balanced voltage levels. If the flying capacitors are not balanced, the switching voltage levels will become corrupted and cause increased voltage stresses, current ripple, and harmonic distortion at the output [9], [10], [26]. Considerable attention has been given to understanding the theory of flying capacitor balancing and developing improved methods for balancing a single-phase, standalone FCML converter.

It has been shown that practical FCML converters exhibit natural balancing [12], [27]–[29]. In this paper, we define natural balancing as the process in which the power losses in the converter gradually balance the flying capacitors to their ideal values. Ideal odd-level FCML converters have been shown to exhibit steady-state indeterminacy, which leads to an increased sensitivity of flying capacitor voltages to parasitic losses and timing imperfections [30]. Therefore, natural balancing can be less reliable, especially when losses are low. Moreover, the variable and nonlinear nature of natural balancing makes it difficult to predict the steady-state flying capacitor voltage imbalance and to size the component ratings [31]–[33].

Many other methods of balancing flying capacitors have been developed, some of which are shown in Fig. 1. Perhaps the most prominent is active balancing, where the flying capacitor voltages are sensed or estimated and then balanced through an active intervention such as adjusting the phase shift or duty cycles of the switches [34]-[37]. This is a flexible and robust technique that is applicable in many FCML converters. However, since active balancing requires additional sensing circuitry and more complex control, it becomes challenging to implement as the number of levels, the switching frequency, or the control bandwidth increase [32], [37]. Other approaches such as balance boosters [13], optimizing the switching sequence [27], [38], [39], or simply choosing an even number of levels [33] seek to improve the passive balancing of FCML converters. Here, we define passive balancing as any balancing mechanism that does not use active control to sense and adjust the flying capacitor voltages. Therefore, natural balancing is a type of passive balancing.

In addition to the practical methods used to balance FCML converters, the underlying theory of how flying capacitors are balanced can be divided into two broad categories: i) dynamic, which describes how FCML converters dynamically balance (or fail to do so) from an initial imbalance [9], [10], [27], and ii) steady-state, which describes the flying capacitor imbalance that persists at steady-state due to external unbalancing mechanisms. In particular, while much early FCML balancing research focuses on dynamic behavior, [40] studies the existence of steady-state imbalances and examples of practical non-idealities that can cause them.

B. Using Coupled Inductors to Balance FCML Converters

One recent advance is the use of coupled inductors to balance multiphase FCML converters in dynamic [1] and steady-state conditions [2], and with multiple phases and levels [3]. By coupling the inductor currents of multiple interleaved FCML converters, the flying capacitors of one phase can compensate the imbalances of another and passively balance the system. This offers several advantages over other means of

balancing: i) The FCML converter system naturally inherits the benefits of coupled inductors in current ripple reduction and faster transient response; ii) Coupled inductors provide lossless flying capacitor voltage balancing without any additional components or changes to the switching scheme that is much stronger than natural balancing in most practical converters; iii) Coupled inductor balancing scales well to higher power levels, large numbers of levels, and higher switching frequencies since there is no need to sense or actively adjust the flying capacitor voltages. However, no systematic analysis has been presented to quantitatively explain the balancing mechanisms of coupled inductors and to explore their applicability and limitations.

C. Contributions of this Work

This paper systematically investigates the mechanisms, applicability, and limitations of coupled inductor balancing of FCML converters. The main contributions are:

- We develop, for the first time, a systematic modeling framework for quantitatively describing the balancing behavior of coupled inductor FCML converters. The models and methods scale well to an arbitrary number of levels, number of phases, and switching pattern.
- We compare coupled inductor balancing to other common techniques such as active balancing and demonstrate its advantages in cost, strength, and flexibility.
- We analyze the limitations of scaling the technique to an arbitrary number of levels and phases, and explore the scenarios when the balancing mechanisms may fail. Balancing with partially coupled inductors is discussed, including desirable regions of coupling to maximize robustness.
- While this paper deals mainly with coupled inductor balancing, the modeling methods and framework are broadly applicable to other FCML converter balancing mechanisms.

The rest of the paper is organized as follows: Section II reviews the background of FCML converters and coupled inductors. Section III explains the fundamental balancing mechanism of coupled inductors. Section IV derives a systematic mathematical framework for studying coupled inductor balancing and to determine which converters coupled inductors can balance. Section V finds the limitations of coupled inductor balancing with regards to the number of phases, levels, and coupling ratio. Section VI verifies the theoretical results using a four-phase, three-level FCML converter and a two-phase, five-level FCML converter. Section VII compares coupled inductor balancing to other common techniques including active balancing, natural balancing, and even-level selection. General design guidelines for coupled inductor FCML converters to minimize capacitor voltage imbalances are reviewed. Finally, we summarize our main findings in Section VIII.

II. FCML Converters with Coupled Inductors

Figure 2 shows a two-phase, three-level FCML converter with coupled inductors used as the canonical cell for presenting the analytical framework. The two phases each have

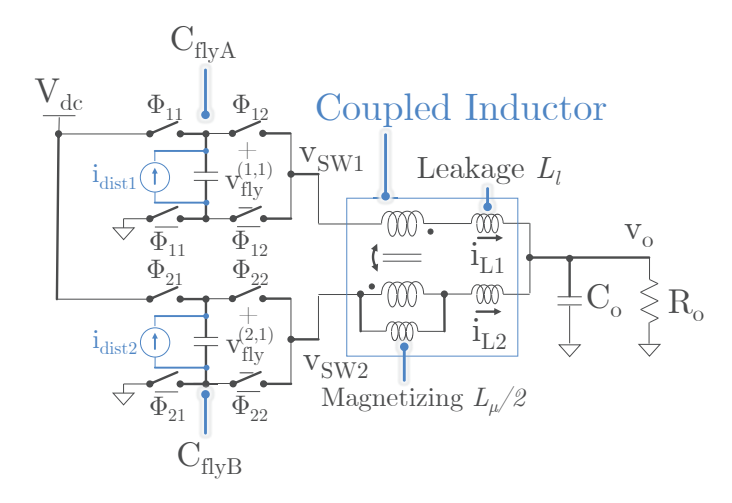


Fig. 2. Schematic of a two-phase, three-level FCML converter with coupled inductors parameterized by the leakage (L_l) and magnetizing (L_μ) inductance. The current sources i_{dist1} and i_{dist2} model mechanisms unbalancing the flying capacitors, such as timing or duty cycle mismatches.

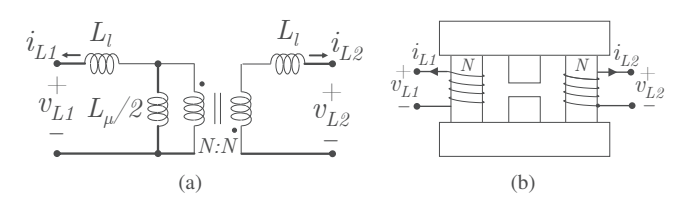


Fig. 3. (a) Schematic and (b) diagram of a two-phase coupled inductor parameterized using leakage and magnetizing inductance.

two pairs of switches operated as complementary pairs to prevent shorting. The switches signals are labelled as Φ_{xy} , where x is the phase number and y orders the switches in one phase with y=1 being closest to the input side. Each phase has a flying capacitor, labeled $C_{\rm fly1}$ and $C_{\rm fly2}$, which ideally have voltages equal to half the input voltage $V_{\rm dc}$ such that the switch node voltages can be $0, \frac{V_{\rm dc}}{2},$ or $V_{\rm dc}$ depending on the switch connections. The phases are coupled by a two-phase coupled inductor, which is also illustrated in Fig. 3. The coupled inductor is parameterized using a transformer model and its leakage and magnetizing inductance, L_l and L_μ . Additional background on multiphase coupled inductors and models used in this paper can be found in Appendix I.

Fig. 4 shows the switching waveforms of the converter, with the switch states and capacitor charge/discharge states detailed in Table I. Both of the individual FCML converter phases are switched using phase-shifted pulse width modulation (PS-PWM), which means the switch pairs in one phase are operated with a duty cycle of d and phase shifted by 180° to distribute the switching actions evenly in the switching period T. The two phases are then themselves interleaved with a phase shift of 90° . The result of this dual interleaving is four evenly interleaved switch pulses, labelled pulse (1) through pulse (4) in Fig. 4. For higher numbers of phases or levels in the FCML converter, the switches are similarly interleaved such that the switching events are always uniformly distributed in a cycle.

During pulse (1), phase #1 connects V_{dc} to v_{SW1} through C_{fly1} and charges the flying capacitor. During pulse (2),

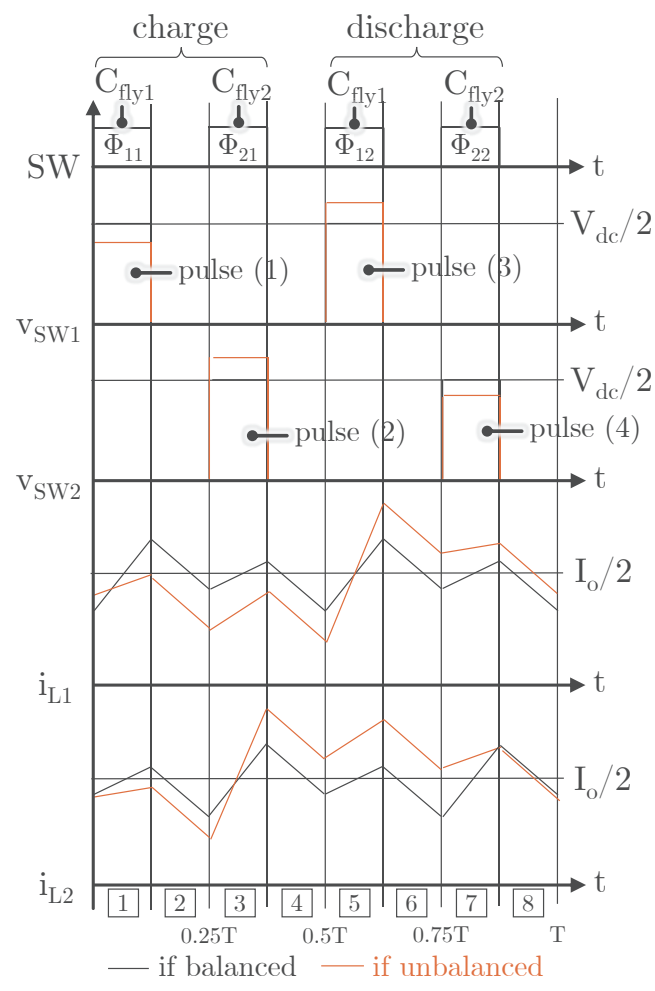


Fig. 4. Switching waveforms of the two-phase, three-level FCML converter in Fig. 2 with PS-PWM and d=0.125. If the flying capacitors are imbalanced (illustrated with a positive imbalance on phase #1 and a negative imbalance on #2), the current ripple is increased.

TABLE I SWITCH AND FLYING CAPACITOR STATES FOR TWO-PHASE, THREE-LEVEL FCML CONVERTER WITH d=0.125

Sub-period	1	2	3	4	5	6	7	8
Start time t	0	$\frac{T}{8}$	$\frac{T}{4}$	$\frac{3T}{8}$	$\frac{T}{2}$	$\frac{5T}{8}$	$\frac{3T}{4}$	$\frac{7T}{8}$
Φ_{11}	1	0	0	0	0	0	0	0
Φ_{21}	0	0	0	0	1	0	0	0
Φ_{21}	0	0	1	0	0	0	0	0
Φ_{22}	0	0	0	0	0	0	1	0
C_{flyA}	chg	-	-	-	dischg	-	-	-
C_{flyB}	-	-	chg	-	-	-	dischg	-

phase #2 connects $V_{\rm dc}$ to v_{SW2} through $C_{\rm fly2}$ and charges the flying capacitor. Pulses (3) and (4) connect the switch nodes to ground through the flying capacitors in the opposite direction, which discharges them. Since the ideal voltage of the flying capacitors is $\frac{V_{\rm dc}}{2}$, each of the four switch node voltage pulses are ideally at $\frac{V_{\rm dc}}{2}$.

With uncoupled inductors, the current in each phase i_{L1} and i_{L2} will ramp based only on the voltage applied to the same coil. Only natural balancing is in effect. When the

inductors are coupled, the currents also ramp depending on the voltage of the other phase. This happens because of the shared magnetic flux paths as shown in Fig. 3(b). To quantify the amount of coupling between the phases, we define the inductive relationships between the phases as

$$\begin{bmatrix} \frac{\mathrm{d}i_{L1}}{\mathrm{d}t} \\ \frac{\mathrm{d}i_{L2}}{\mathrm{d}t} \end{bmatrix} = \underbrace{\begin{bmatrix} 1/L_{\mathrm{same}} & 1/L_{\mathrm{cross}} \\ 1/L_{\mathrm{cross}} & 1/L_{\mathrm{same}} \end{bmatrix}}_{f_{c}-1} \begin{bmatrix} v_{L1} \\ v_{L2} \end{bmatrix}, \tag{1}$$

where the inductor voltages and currents are labelled in Fig. 3(a). Matrix \mathcal{L}^{-1} is the inverse of the inductance matrix \mathcal{L} in $\mathbf{v_L} = \mathcal{L} \frac{d\mathbf{i_L}}{d\mathbf{t}}$ describing the induced voltages in each coil due to changing coil currents. \mathcal{L} is traditionally parameterized by the self and mutual inductances [24]. The formulation in eq. (1) is inverted, with changing currents expressed as a function of applied voltages: $\frac{d\mathbf{i_L}}{d\mathbf{t}} = \mathcal{L}^{-1}\mathbf{v_L}$. To avoid confusion with the self and mutual inductances, we define the *same inductance* ($L_{\rm same}$) describing the resulting current ramp if a voltage is applied to the same winding, and the *cross inductance* ($L_{\rm cross}$) describing the current induced in one phase if the other has a voltage applied to it. According to [24], $L_{\rm cross}$ and $L_{\rm same}$ are functions of the mutual and leakage inductance L_u and L_l :

$$L_{\text{cross}} = \left(\frac{M-1}{\mu} + M\right) L_l,\tag{2}$$

$$L_{\text{same}} = \frac{\mu}{M - 1 + \mu} \left(\frac{M - 1}{\mu} + M \right) L_l, \tag{3}$$

where M is the number of phases and $\mu=\frac{L_{\mu}}{L_{l}}$ is the coupling ratio. $L_{\rm cross}$ is always greater than or equal to $L_{\rm same}$. When $\mu\to\infty$, the inductors becoming fully coupled and $L_{\rm cross}=L_{\rm same}=ML_{l}$, indicating that applied phase voltages have equal influence on all phase current.

Fig. 4 shows the inductor current waveforms in the two-phase example that are typical of a coupled inductor system. For example, the current in phase 2 increases during subperiod #1 despite the fact that the voltage on its coil is $-V_o$ during this time. This is because the first coil has a positive voltage and is coupled to it. The current in phase 2 will not necessarily increase during sub-period #1 depending on the coupling ratio [24], but its slope will always be greater than if there was no coupling.

Because a voltage applied on either coil ramps the current in both, the current ripple frequency is doubled from usual and the ripple is reduced. Increasing the coupling ratio increases the effect that the voltage on one coil has on the current in the other. A fully coupled inductor, where the flux in each phase is identical, would have $L_{\rm cross} = L_{\rm same}$ and the same current (both dc current and ac ripple) in both phases. With tight coupling, it is important to switch all phases with proper phase shifting, as the core will present a low inductance if only one phase is switched and be prone to saturation.

If the flying capacitor voltages are not equal to $V_{\rm dc}/2$, they are unbalanced. Fig. 4 illustrates this for the case where flying capacitor #1 has a positive imbalance and flying capacitor #2 has a negative imbalance. In this case, the switch node pulses have voltages above and below the ideal level, which increases

the current ripple. Moreover, the voltage stress on the switches is increased. This is why it is important to ensure the flying capacitor voltages remain balanced.

Later sections of this paper deal with FCML converters with more phases and levels. We define the number of phases as M and the number of flying capacitors in each phase as K. Each phase is therefore a (K+2)-level FCML converter since the number of possible switching levels is always two more than the number of flying capacitors. We denote the flying capacitor voltages as $v_{\rm fly}^{\rm (phase\ \#m,\ cap\ \#k)}$, or for brevity, $v_{\rm fly}^{\rm (m,k)}$, where $m=1,\ldots,M$ and $k=1,\ldots,K$ are the indices identifying the phase and capacitor. The capacitor closest to the input source has the index k=1. The ideally balanced flying capacitor voltages in this case are

$$v_{\text{fly, balanced}}^{(\text{#m, #k})} = V_{\text{dc}} \frac{K+1-k}{K+1},$$
 (4)

which are the voltages that result in equal voltage stresses on all switches and switching levels that are evenly spaced between 0 and $V_{\rm dc}$.

III. FUNDAMENTAL PRINCIPLES OF COUPLED INDUCTOR FCML CONVERTER BALANCING

In this section, we present a feedback framework to explain the mechanisms of coupled inductor voltage balancing for FCML converters. In the context of this paper, we define *voltage balancing* as the flying capacitor voltages reaching steady-state values, and we are interested in understanding the mismatches between these steady-states and the nominal capacitor voltages. We start by formally reviewing small-signal modelling of FCML converter balancing. Then, we show how the losses in a FCML converter will naturally force the system into a steady-state, regardless of if the inductors are coupled or uncoupled, then compare the resulting steady-state values in the uncoupled and coupled cases.

A. Small-Signal Modeling of FCML Converter Balancing

In this section, we formalize the small-signal modelling principles used to develop the feedback models in the proceeding sections. First, we examine the schematic of the three-level converter in Fig. 5. The state variables are the inductor current i_L and the flying capacitor voltage $v_{\rm fly}$. These state variables can be further divided by superposition into balanced and unbalanced components. This division simplifies the analysis since only the unbalanced components, the flying capacitor voltage imbalance $\tilde{v}_{\rm fly}$ and the inductor current imbalance \tilde{i}_L , are relevant to balancing analysis. The large-signal load current I_o , the ideally balanced voltage flying capacitor, $V_{\rm dc}/2$, and the switching ripple (which we assume to be negligible) are components of normal operation that can be ignored. Therefore, each flying capacitor voltage is written as

$$v_{\rm fly}^{(m,k)} = v_{\rm fly,\;balanced}^{(m,k)} + \tilde{v}_{\rm fly}^{(m,k)}, \tag{5}$$

where the balanced level is defined in eq. (4). Fig. 6 shows the switching waveforms of the three-level converter. We wish to relate the imbalance voltage, power loss, and current in the flying capacitor. In our analysis, we assume the power loss

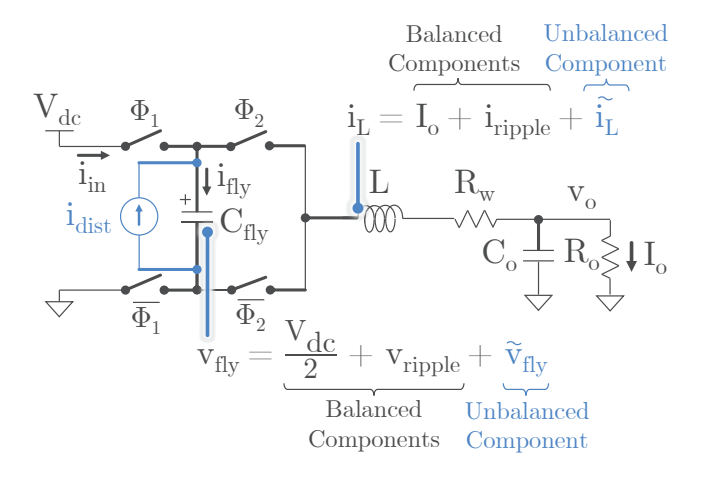


Fig. 5. Schematic of a three-level FCML converter with separation of balanced and unbalanced components of state variables.

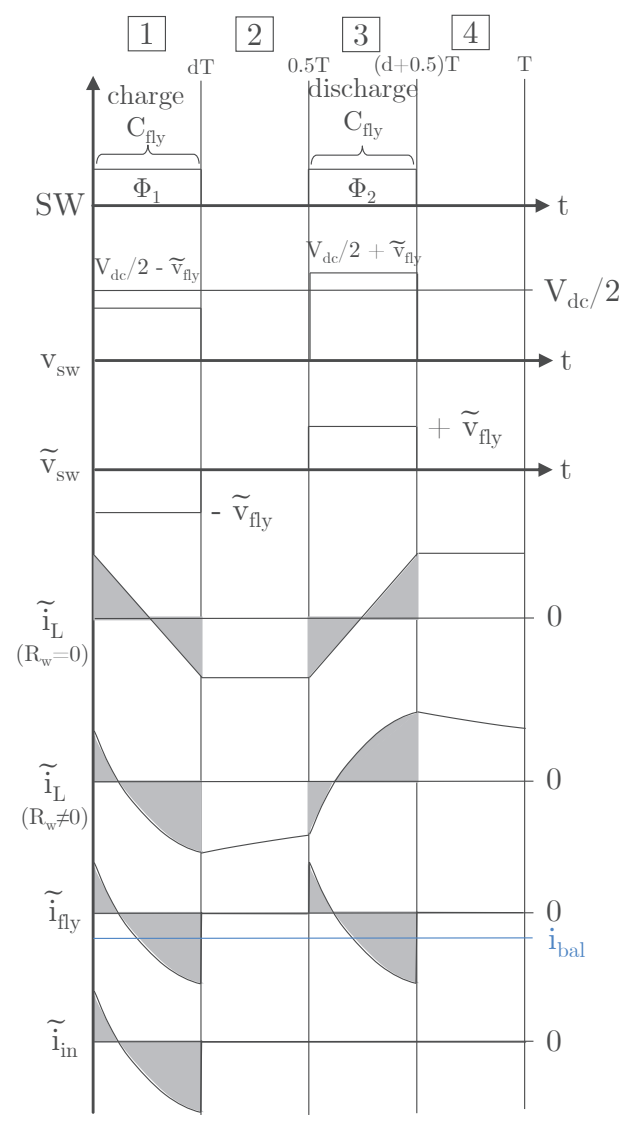


Fig. 6. Switching waveforms of a single-phase three-level FCML converter. The unbalanced component of the switch node voltage causes a perturbation of the inductor current, $\tilde{i_L}$. If the resistance R_w is zero, the inductor current perturbation ramps linearly and causes no charge transfer in the flying capacitor. If the resistance is nonzero, the inductor current ramps exponentially and there is a net charge transfer, thus causing lossy natural balancing.

comes from the resistance in series with the inductor R_w . First, we analyze how an imbalance in the flying capacitor affects power transfer in the converter. There are four sources and sinks of power in the converter in Fig. 5: i) power dissipated in the resistance, ii) power input from the source $V_{
m dc}$, iii) power output to the load, and iv) power that charges the flying capacitor. First, we compute the loss that an unbalanced flying capacitor causes in the resistor. Fig. 6 shows the switching waveforms of the three-level converter. By superposition, the imbalanced component of the flying capacitor voltage, $\tilde{v}_{\rm fly}$, is applied to the switch node twice in alternating directions every period. This induces an imbalanced component of the inductor current ripple \tilde{i}_L . Assuming the flying capacitor is large enough such that the flying capacitor voltage does not change appreciably during a switching period, induced current is symmetric across t = 0.5T and has zero mean. This assumption is valid because the flying capacitors must be sized large enough to minimize the ripple at maximum load and protect the switches. Averaging over a switching period, the unbalanced inductor current causes an average power loss in the resistance R_w

$$\langle P_{R_w} \rangle = \langle R_w i_L^2 \rangle = \langle R_w (I_o + \tilde{i_L})^2 \rangle$$

$$= R_w I_o^2 + R_w \langle \tilde{i_L}^2 \rangle + R_w I_o \langle \tilde{i_L} \rangle^0$$

$$= R_w I_o^2 + R_w \langle \tilde{i_L}^2 \rangle. \tag{6}$$

Here, $\langle x(t) \rangle = \frac{1}{T} \int_0^T x(t) \, \mathrm{d}t$ represents the average over a switching period. Because the FCML converter switches the flying capacitor in alternating directions symmetrically every period, the inductor imbalance current is symmetric about zero and has zero mean, meaning the loss components from the large- and small- signal current are independent. Next, the output power is

$$P_o = I_o(dV_{dc} - R_w I_o), \tag{7}$$

assuming the output capacitor is very large such that the output voltage is constant. The flying capacitor current is equal to the inductor current with alternating directions as shown in Fig. 6. The power transferred to the flying capacitor is

$$\langle P_{\text{fly}} \rangle = \left(\frac{V_{\text{dc}}}{2} + \tilde{v}_{\text{fly}}\right) \langle \tilde{i}_{\text{fly}} \rangle.$$
 (8)

Finally, power comes from the input source. The input current sees the same imbalance current as the flying capacitor during $0 < t \le dT$. The flying capacitor current during $0.5T < t \le (d+0.5)T$ is identical to $0 < t \le dT$, but the input source is not connected during this time. Therefore, the average current from the source is equal to the average capacitor current divided by two. The average power from the source is

$$\langle P_{\rm in} \rangle = dV_{\rm dc}I_o + V_{\rm dc}\frac{\langle \tilde{i}_{\rm fly} \rangle}{2}.$$
 (9)

By conservation of energy, the average power of all sources and sinks sums to zero:

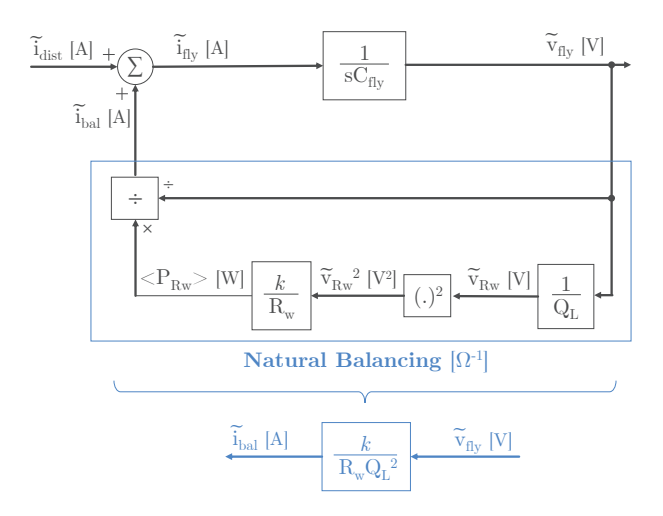


Fig. 7. Feedback diagram of natural balancing in standard FCML converter, where power losses provide the balancing action.

$$\langle P_{\rm in} \rangle - P_o - \langle P_{\rm fly} \rangle - \langle P_{R_w} \rangle = 0$$

$$\underbrace{\frac{dV_{\rm dc} I_o + V_{\rm dc} \langle \tilde{i}_{\rm fly} \rangle / 2}_{\langle P_{\rm in} \rangle} - \underbrace{\left(I_o dV_{\rm dc} - R_w I_o^2\right)}_{P_o}}_{P_o}$$

$$-\underbrace{\left(\frac{V_{\rm dc}}{2} + \tilde{v}_{\rm fly}\right) \langle \tilde{i}_{\rm fly} \rangle}_{\langle P_{\rm fly} \rangle} - \underbrace{\left(R_w I_o^2 + R_w \langle \tilde{i}_L^2 \rangle\right)}_{\langle P_{R_w} \rangle} = 0$$

$$\rightarrow \tilde{v}_{\rm fly} \langle \tilde{i}_{\rm fly} \rangle - R_w \langle \tilde{i}_L^2 \rangle = 0$$

$$\rightarrow \tilde{i}_{\rm bal} := \langle \tilde{i}_{\rm fly} \rangle = -\frac{R_w \langle \tilde{i}_L^2 \rangle}{\tilde{v}_{\rm fly}}. \tag{10}$$

The average current into the flying capacitor, which we define here as the balancing current \tilde{i}_{bal} , is dependent only on the "small-signal" loss in the resistor $R_w \left< \tilde{i_L}^2 \right>$ and the flying capacitor voltage. It is not dependent on the large-signal input voltage or load current. This happens because for every unit of charge taken from the flying capacitor, a proportional unit is taken from the input source. In other words, the small-signal power loss affects the small-signal flying capacitor voltage, while the large-signal flying capacitor voltage is taken care of by the input source. The balancing effect always reduces the flying capacitor imbalance. Since the power loss is always positive, if the flying capacitor imbalance voltage $\tilde{v}_{\rm fly}$ is positive, $\tilde{i}_{\rm bal}$ is negative and the flying capacitor is discharged by the power loss, and vice versa if the imbalance is negative.

B. Feedback Model of Natural Balancing

We develop a model for natural balancing using the singlephase FCML converter shown in Fig. 5 to compare it to the canonical coupled two-phase case. FCML converters exhibit natural balancing, where flying capacitor imbalance voltages cause increased losses that dissipate the imbalance gradually [9], [10], [12], [26], [41]. For converters without balancing techniques like active balancing, natural balancing is the dominant mechanism that determines the flying capacitor voltages.

Assuming the inductor resistance R_w provides the loss source, the "small-signal" power loss $\left\langle \tilde{P}_{R_w} \right\rangle$, considering only the unbalanced state variables, is

$$\left\langle \tilde{P}_{R_w} \right\rangle = \frac{\gamma}{R_w Q_L^2} \tilde{v}_{\rm fly}^2,\tag{11}$$

where $\gamma=\frac{d^2(3-4d)\pi^2}{3}$ is a scaling factor depending on the duty cycle and $Q_L=\frac{\omega_{\rm Sw}L}{R_w}$ is the quality factor of the inductor at the switching frequency. The details of this calculation are contained in Appendix II. The power loss is equal to the approximate imbalance voltage over the resistor $\frac{\tilde{v}_{\rm fly}}{Q_L}$ squared, divided by the winding resistance R_w and scaled by γ . As proven in Section III-A (and verified in Appendix II), this power loss causes an effective balancing current

$$\tilde{i}_{\text{bal}} = \frac{\left\langle \tilde{P}_{R_w} \right\rangle}{\tilde{v}_{\text{fly}}} = \frac{\gamma}{R_w Q_L^2} \tilde{v}_{\text{fly}}.$$
 (12)

Equation (12) relates the balancing current to the power loss, and by extension, the imbalance voltage. Using these equations, we construct the feedback model of natural balancing shown in Fig. 7. The flying capacitor is modelled as an integrator of current that produces an imbalance $\tilde{v}_{\rm fly}$ which feeds back via natural balancing to counteract external disturbances modelled using $\tilde{i}_{\rm dist}$. The flying capacitor imbalance voltage $\tilde{v}_{\rm fly}$ induces an average power loss $\langle P_{R_w} \rangle$ depending on the quality factor of the inductor Q_L .

The feedback diagram emphasizes the fundamental problems with natural balancing: it relies on large converter losses to be effective. The steady-state gain from disturbance to imbalance, which we compute by setting $\tilde{i}_{\text{dist}} = -\tilde{i}_{\text{bal}}$, is

$$\frac{\tilde{v}_{\text{fly}}}{\tilde{i}_{\text{dist}}}\Big|_{\text{steady-state}} = \frac{Q_L^2 R_w}{\gamma}.$$
 (13)

If the quality factor Q_L of the inductor is high, the gain from imbalance voltage to balancing current will be low, leading to weak balancing capability.

C. Feedback Model of Coupled Inductor Balancing

Coupled inductor balancing uses a fundamentally different mechanism to natural balancing. Fig. 8 illustrates the balancing mechanism in a feedback model for a two-phase FCML converter with coupled inductors. An imbalance voltage on either phase will induce a current in the other through the coupled inductors. We show that in periodic steady state, coupled inductors create a negative feedback loop through the cross inductance $L_{\rm cross}$ to greatly mitigate the voltage imbalance created by an external disturbance. This mechanism is significantly more effective than the lossy mechanism of natural balancing because its gain is much higher.

Fig. 9 details the coupled inductor feedback loop. Through the coupled currents, the imbalance voltage of phase #2 can compensate for the disturbance current in phase #1 and vice versa. Both phase imbalances induce currents in the other with slope $^1/L_{\rm cross}$ and scaled by a timing factor derived in Appendix II. In the $0 < d < \frac{1}{4}$ case, this timing factor has magnitude d^2T because the induced current ramps up for dT and then the balanced flying capacitor is connected for duration dT, so the average balancing current is scaled by $dT \times dT/T = d^2T$.

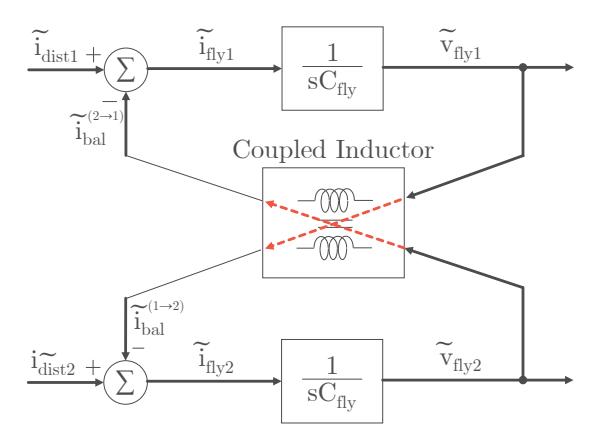


Fig. 8. Feedback diagram of two-phase, three-level FCML converter balanced by coupled inductors.

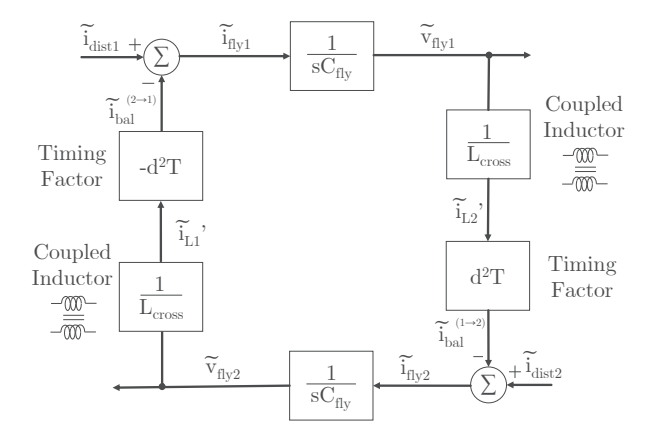


Fig. 9. Detailed feedback balancing diagram of coupled inductor FCML converter where an imbalance voltage on phase #1 or #2 compensates for a disturbance on phase #2 or #1 respectively when $0 < d < \frac{1}{4}$.

The closed-loop transfer functions from $\{i_{\text{dist1}}, i_{\text{dist2}}\}$ to $\{\tilde{v}_{\text{fly1}}, \tilde{v}_{\text{fly2}}\}$, which are computed by dividing the forward gain by the loop gain, are

$$\begin{bmatrix} \tilde{v}_{fly1} \\ \tilde{v}_{fly2} \end{bmatrix} \bigg|_{coupled} = \begin{bmatrix} \frac{\frac{1}{sC_{fly}}}{1 - (\frac{d^2T}{L_{cross}} \frac{1}{sC_{fly}})^2} & -\frac{d^2T}{L_{cross}} (\frac{1}{sC_{fly}})^2 \\ \frac{d^2T}{L_{cross}} (\frac{1}{sC_{fly}})^2 & \frac{1}{sC_{fly}} \\ \frac{d^2T}{L_{cross}} (\frac{1}{sC_{fly}})^2 & \frac{1}{sC_{fly}} \\ 1 - (\frac{d^2T}{L_{cross}} \frac{1}{sC_{fly}})^2 & \frac{1}{1 - (\frac{d^2T}{L_{cross}} \frac{1}{sC_{fly}})^2} \end{bmatrix} \begin{bmatrix} \tilde{i}_{dist1} \\ \tilde{i}_{dist2} \end{bmatrix}.$$
(14)

The steady state dc gain of the system when $s \to 0$ is

$$\begin{bmatrix} \tilde{v}_{\text{fly1}} \\ \tilde{v}_{\text{fly2}} \end{bmatrix} \bigg|_{\text{steady-state, coupled}} = \begin{bmatrix} 0 & \frac{L_{\text{cross}}}{d^2 T} \\ -\frac{L_{\text{cross}}}{d^2 T} & 0 \end{bmatrix} \begin{bmatrix} \tilde{i}_{\text{dist1}} \\ \tilde{i}_{\text{dist2}} \end{bmatrix}. \quad (15)$$

The negative symbol is determined by the order of the switching order of phase #1 and phase #2 in a cycle. This equation confirms that the impact of coupled inductor balancing is only determined by $L_{\rm cross}$, d, and T and is independent from resistance R_w .

We now compare the imbalances in the uncoupled (13) and coupled (15) cases. If the same disturbance is applied to both converters, the ratio of the steady-state imbalance voltage between the coupled and uncoupled converter when $0 < d < \frac{1}{4}$ is

$$\left| \frac{\tilde{v}_{\text{fly, coupled}}}{\tilde{v}_{\text{fly, uncoupled}}} \right| = \frac{L_{\text{cross}}}{d^2 T} \times \frac{\gamma}{Q_L^2 R_w}. \tag{16}$$

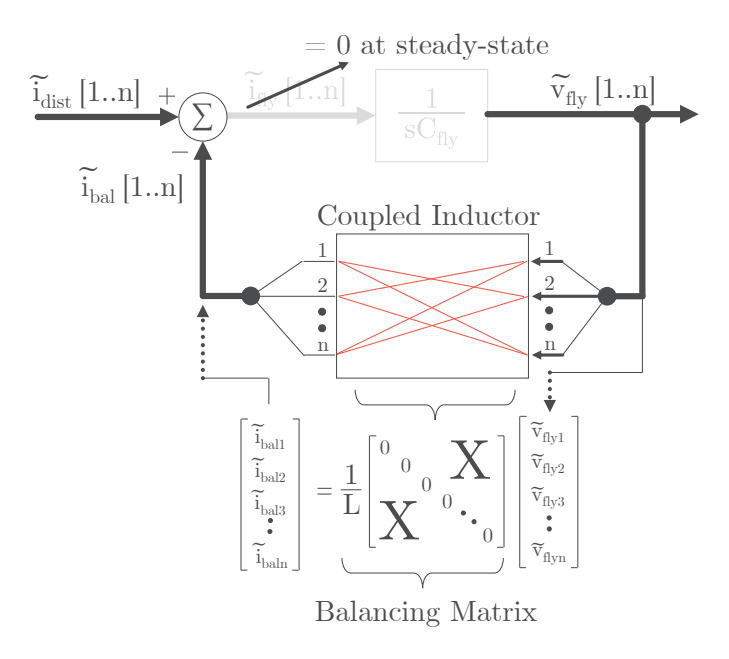


Fig. 10. Generalized feedback balancing diagram for an FCML converter with an arbitrary number of flying capacitors.

In a tightly coupled inductor design, $L_{\rm cross}$ is usually much smaller than $L_{\rm uncoupled}$. In this case, the imbalance of the coupled inductor system is much smaller than the uncoupled system. As we seek to reduce converter losses by minimizing R_w and maximizing the quality factor of the inductor Q_L , the relative strength of coupled inductor balancing becomes more pronounced.

IV. A GENERALIZED MODELING FRAMEWORK FOR STEADY-STATE BALANCING ANALYSIS

This section develops a generalized framework for analyzing coupled inductor balancing for converters with an arbitrary number of phases and levels. This model is used to determine the applicability and limitations of balancing with coupled inductors in multiphase FCML converters.

A. Feedback Model of Coupled Inductor Balancing for Arbitrary FCML Converter Size

First, we extend the feedback models in Section III-C to any FCML converter size. Consider a converter with M phases and (K+2)-levels with a total of n=MK flying capacitors in the system. Fig. 10 shows the generalized feedback diagram. The bold connections are signal buses for all the n flying capacitor voltages and currents. With n flying capacitors, each flying capacitor voltage imbalance induces a current that balances up to n-1 other capacitors through the coupled inductors. This is represented by the balancing matrix in Fig. 10. The balancing matrix describes the effective balancing current or charge that is induced in every flying capacitor as a result of the imbalance voltages in all the other flying capacitors. The balancing matrix is important, because it determines whether or not the coupled inductors can counteract the disturbance currents.

By inspection of Fig. 10, we define the following multiphase FCML balancing criterion: the converter is balanced if the flying capacitor imbalance voltages can balance an arbitrary set of disturbance currents. This criterion is met if the balancing matrix is full rank. Having a full-rank balancing matrix means that the system only has one unique periodic-steady-state and will not oscillate between two or more states. This property and the generalized feedback diagram are used throughout the rest of this paper.

If the system is to reach a steady state with a persistent disturbance current (\tilde{i}_{dist}) at each phase, the disturbance current in every capacitor needs to be canceled by the total cross-phase balancing current (\tilde{i}_{bal}) introduced by the coupled inductors:

$$\tilde{\mathbf{i}}_{\text{bal}} + \tilde{\mathbf{i}}_{\text{dist}} = \mathbf{0}. \tag{17}$$

Assuming the system is periodic with T, eq. (17) can be rewritten in terms of charges instead of currents as

$$\mathbf{Q}_{\text{bal}} + \mathbf{Q}_{\text{dist}} = \mathbf{A}\tilde{\mathbf{v}}_{\text{flv}} + \mathbf{Q}_{\text{dist}} = \mathbf{0},\tag{18}$$

where $\tilde{\mathbf{v}}_{fly}$ is a vector of all the flying capacitor voltage imbalances. The balancing matrix \mathbf{A} relates the flying capacitor imbalance voltages to the resulting balancing charges on the other flying capacitors and depends on the switching order, duty cycle, and coupling ratio.. We can find the steady-state capacitor imbalances in terms of the disturbance charge if and only if \mathbf{A} is invertible.

$$\tilde{\mathbf{v}}_{\text{fly}} = -\mathbf{A}^{-1}\mathbf{Q}_{\text{dist}}.\tag{19}$$

In summary, the balancing matrix A describes the amount of balancing charge induced in each phase by the others through the coupled inductor. If A is full rank, then an arbitrary disturbance can be canceled out by the coupled inductor and the system is balanced and will reach a steady-state computer by eq. (19).

B. Balancing with an Arbitrary Number of Phases

This section shows that an M-phase coupled inductor can balance the flying capacitors of any even number of three-level FCML converter phases. To prove this, we compute the balancing matrix and show that it is full rank. We begin with the case when the duty cycle is in the region $0 < d \leq \frac{1}{2M}$. First, we consider if the flying capacitor of phase #1 has a positive imbalance, $\tilde{v}_{\rm fly}^{(1,1)}$. This imbalance is applied negatively and positively to the switch node once per period, as shown in Fig. 11 for a four-phase example. This induces an imbalance inductor current $i_{\rm L}^{\#1 \to \#2, \#3, \#4}$ in the other three phases. When the other three flying capacitors are connected, they receive a charge transfer labelled $Q_{\rm bal}^{(1,1)\to(2,1)}$, $Q_{\rm bal}^{(1,1)\to(3,1)}$, and $Q_{\rm bal}^{(1,1)\to(4,1)}$. Therefore, the charge transfer induced by phase #1 in the other flying capacitors is

$$Q_{\text{bal}}^{(1,1)\to(m,1)} = -\frac{(dT)^2}{L_{\text{cross}}} \tilde{v}_{\text{fly}}^{(1,1)}, \tag{20}$$

for $m=2,\ldots,M$. Thus, a positive voltage imbalance on flying capacitor (1,1) causes a uniform negative charge transfer on the other flying capacitors. We calculate the remaining entries of the balancing matrix in a similar way. All the flying

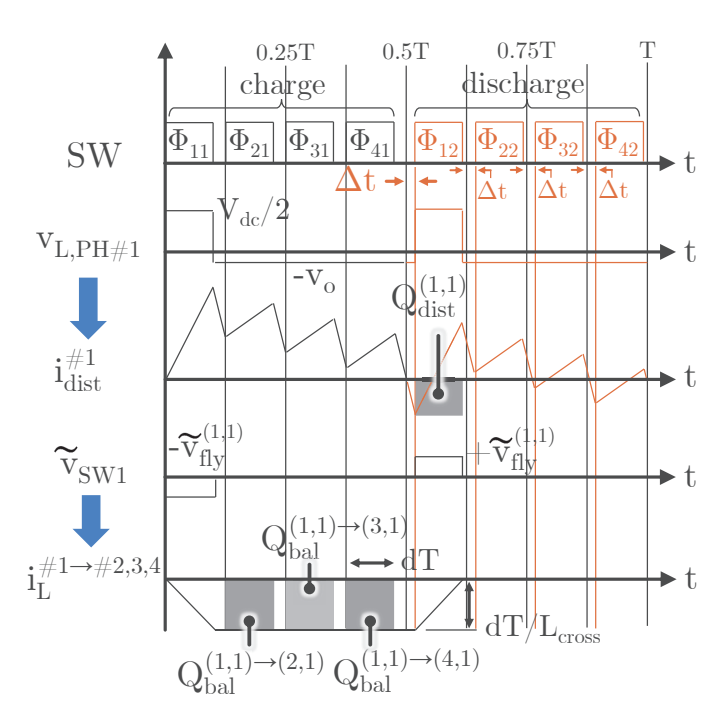


Fig. 11. Switching waveforms of four-phase, three-level FCML converter with the second set of switches delayed by a disturbance. The disturbance charge caused by the delay and the balancing charge caused by the other flying capacitors must cancel out at steady-state.

capacitors cause the same charge transfer magnitude in the other phases; the only difference is the sign, which will be positive or negative depending on whether the target flying capacitor is in its charging or discharging phase. The resulting charge transfers are

$$Q_{\text{bal}}^{(m_{\text{s}},1)\to(m_{\text{t}},1)} = \begin{cases} -\frac{(dT)^2}{L_{\text{cross}}} \tilde{v}_{\text{fly}}^{(m_{\text{s}},1)} & m_{\text{s}} < m_{\text{t}} \\ +\frac{(dT)^2}{L_{\text{cross}}} \tilde{v}_{\text{fly}}^{(m_{\text{s}},1)} & m_{\text{s}} > m_{\text{t}} \\ 0 & m_{\text{s}} = m_{\text{t}} \end{cases}$$
(21)

where $m_{\rm s}=1,\ldots,M$ is the "source" flying capacitor that is unbalanced, and $m_{\rm t}=1,\ldots,M$ is the "target" flying capacitor that receives a charge. From eq. (21), we write the complete balancing matrix that relates the imbalance voltages and balancing currents in matrix form

$$\mathbf{A} = \frac{(dT)^2}{L_{\text{cross}}} \begin{bmatrix} 0 & 1 & 1 & 1 & \cdots & 1 \\ -1 & 0 & 1 & 1 & \cdots & 1 \\ -1 & -1 & 0 & 1 & \cdots & 1 \\ -1 & -1 & -1 & 0 & \cdots & 1 \\ \vdots & \vdots & \vdots & \vdots & \ddots & \vdots \\ -1 & -1 & -1 & -1 & \cdots & 0 \end{bmatrix}$$
(22)

for an M-phase, three-level converter with $d < \frac{1}{2M}$. The main diagonal is zeros, since no flying capacitor induces a net charge transfer in itself. The remaining entries all have the same magnitude and sign determined by the switching order. The flying capacitor voltage imbalance will reach a steady state if \mathbf{A} is invertible. As shown in Appendix III, \mathbf{A} is invertible for an even M, and is non-invertible for an odd M.

Case Study: Time Delay in an Even M-Phase Converter

The prior analysis is applicable to any disturbance. As a case study of how the actual steady-state imbalances would be computed for a specific disturbance, we take a uniform time delay of the second set of switches (the pair further from the input side) of every phase for an even M-phase converter. This disturbance is illustrated in Fig. 11. Because of the time delay Δt , which might be caused by rise/fall times, signal mismatches, etc, the inductor current in each phase ramps down longer before the discharging phase of every flying capacitor. The current in phase #1, $i_L^{\#1}$, is shown as an example. This means that all the flying capacitors charge more than they discharge during every switching period, resulting in a persistent unbalancing current. The disturbance charge, shown by the shaded area under the $i_{\rm dist}^{\#1}$ curve in Fig. 11, is

$$Q_{\rm dist}^{(m,1)} = dT \times \frac{dV_{\rm dc}}{L_l} \Delta t, \tag{23}$$

for m=1...M where L_l is the leakage inductance of the coupled inductor from the transformer model in Fig. 3. Therefore, the complete disturbance vector is

$$\mathbf{Q}_{\text{dist}} = dT \frac{dV_{\text{dc}}}{L_l} \Delta t \begin{bmatrix} 1\\1\\1\\1\\\vdots \end{bmatrix}_{M \times 1}.$$
 (24)

We now plug the disturbance vector into eq. (19) to find the steady-state capacitor voltage imbalances are

$$\tilde{\mathbf{v}}_{\text{fly}} = \begin{bmatrix} \tilde{v}_{\text{fly}}^{(1,1)} \\ \tilde{v}_{\text{fly}}^{(2,1)} \\ \tilde{v}_{\text{fly}}^{(3,1)} \\ \vdots \\ \tilde{v}_{\text{fly}}^{(M,1)} \end{bmatrix} = -\mathbf{A}^{-1} \mathbf{Q}_{\text{dist}} = V_{\text{dc}} \frac{\Delta t}{T} \frac{L_{\text{cross}}}{L_{l}} \begin{bmatrix} 1 \\ -1 \\ 1 \\ \vdots \\ -1 \end{bmatrix}_{M \times 1},$$
(25)

where the inverse of A is computed in Appendix III. The voltage imbalances with coupled inductor balancing are only dependent on the coupling coefficient and not on losses, since loss-based natural balancing is negligible. The magnitudes in all capacitors are equal and the signs are determined by the switching order. One half of the capacitors have positive voltage imbalance, while the other half have negative voltage imbalance. The steady-state imbalance is proportional to $\Delta t/T$ and M. The voltage imbalance also increases with the number of phases. A higher coupling ratio k leads to smaller steady-state voltage imbalances, and if the windings are perfectly coupled, i.e., $\mu \to +\infty$, the minimum steady-state voltage imbalance is

$$\left|\tilde{\mathbf{v}}_{\text{fly}}\right|_{\text{tightly coupled}} \approx V_{\text{dc}} \frac{M\Delta t}{T} \begin{bmatrix} 1\\-1\\1\\\vdots\\-1 \end{bmatrix}_{1 \times M},$$
 (26)

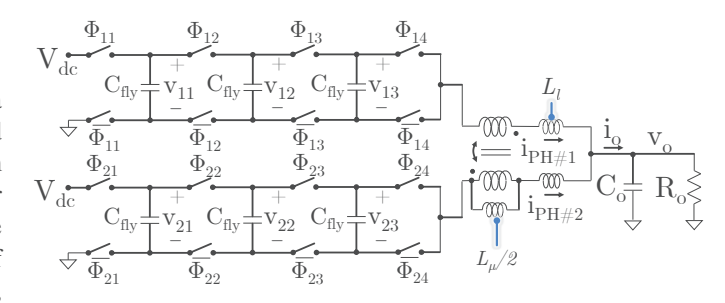


Fig. 12. Schematic of two-phase, five-level FCML converter with coupled inductors. The flying capacitors are numbered by the second index k=1,2,3, where k=1 is closest to the input voltage source.

following from eq. (2). Note that for time delay disturbances, the voltage balancing is also independent of the power level of the FCML converter. For other disturbances, coupled inductor balancing can still be dependent on the load.

We now consider a more general time-shift disturbance when the second set of switches of every converter phase is time-shifted from the first set by Δt positively (lead) or negatively (lag), as in Fig. 11. Appendix III derives the best- and worst- case imbalances for this arbitrary time shift disturbance. In the worst case, all the time shifts are alternating direction and the disturbance vector is

$$\mathbf{Q}_{\text{worst-case}} = dT \frac{dV_{\text{dc}}}{L_l} \Delta t \begin{bmatrix} +1\\-1\\+1\\-1\\\vdots \end{bmatrix}_{M \times 1}, \tag{27}$$

and the largest flying capacitor imbalance is

$$\max \left(\tilde{\mathbf{v}}_{\text{fly}} \right) \big|_{\text{worst-case}} = \frac{(M-1)V_{\text{dc}}\Delta t}{T} \left(\frac{M-1}{k} + M \right). \tag{28}$$

The imbalance scales with M^2 , meaning the balancing becomes weaker as M increases.

C. Balancing with an Arbitrary Number of Levels

This section shows that coupled inductors can balance FCML converters with any finite number of levels. We prove this by computing the balancing matrix for a (K+2)-level converter and showing that it is full rank.

Fig. 12 shows a two-phase, five-level converter with switching waveforms in Fig. 13 for $d < \frac{1}{2(K+1)}$ as an example. The steps required to prove the balancing capabilities of a (K+2)-level converter are similar to Section IV-B. Each flying capacitor imbalance voltage causes balancing charge transfers in the other flying capacitors. The balancing matrix (derived in Appendix IV) is

(26)
$$\mathbf{A}_{(K+2)\text{-levels}} = \begin{bmatrix} 0 & \alpha & \beta & 0 & 0 & \cdots & 0 \\ -\alpha & 0 & \alpha & \beta & 0 & \cdots & 0 \\ -\beta & -\alpha & 0 & \alpha & \beta & \cdots & 0 \\ 0 & -\beta & -\alpha & 0 & \alpha & \cdots & 0 \\ 0 & 0 & -\beta & -\alpha & 0 & \cdots & 0 \\ \vdots & \vdots & \vdots & \vdots & \vdots & \ddots & \vdots \\ 0 & 0 & 0 & 0 & 0 & \cdots & 0 \end{bmatrix}, (29)$$

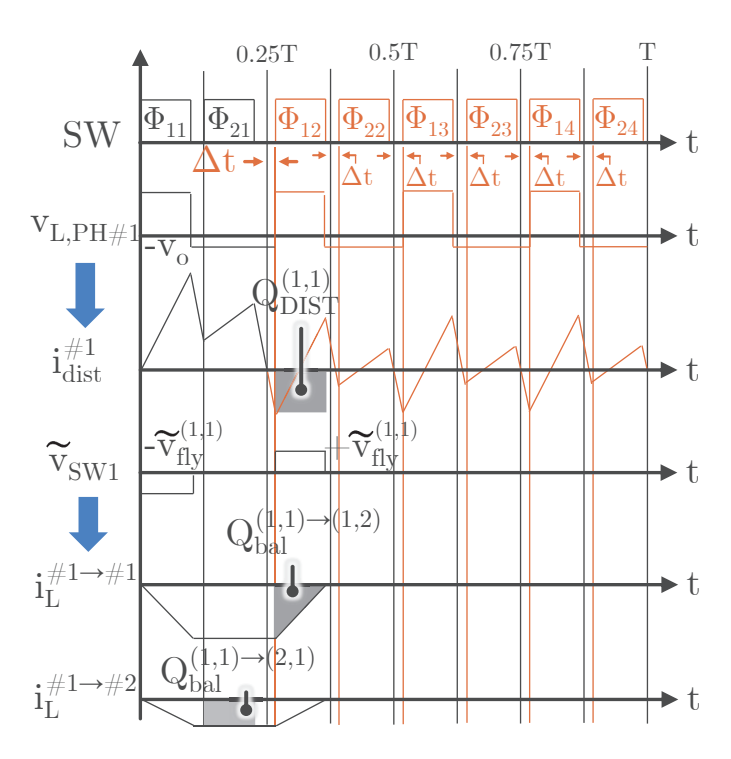


Fig. 13. Switching waveforms of two-phase, five-level FCML converter with time delay disturbance. An imbalance on capacitor #1 of phase #1 will cause a balancing charge on capacitor #2 of phase #1 and capacitor #1 of phase #2.

where $\alpha=\frac{(dT)^2}{L_{\rm cross}}$ and $\beta=\frac{(dT)^2}{2L_{\rm same}}$. The *same* inductance $L_{\rm same}$ appears because there are multiple flying capacitors in the same phase that induce balancing currents in each other. The size is $2K\times 2K$ because each phase has K flying capacitors. The vector of flying capacitor voltages corresponding with eq. (29) is

$$\mathbf{v} = \begin{bmatrix} v_{\text{fly}}^{(1,1)} & v_{\text{fly}}^{(2,1)} & v_{\text{fly}}^{(1,2)} & v_{\text{fly}}^{(2,2)} & \cdots & v_{\text{fly}}^{(1,K)} & v_{\text{fly}}^{(2,K)} \end{bmatrix}^{\text{T}}.$$
(30)

As proven in Appendix IV, $A_{(K+2)\text{-levels}}$ is invertible for any finite number of levels if the coupled inductors are fully coupled ($L_{\text{same}} = L_{\text{cross}}$). In Section V, we treat cases with other duty cycles and phase counts.

Case Study: Time Delay in a Two-Phase, Five-Level Converter

As an example of how the actual steady-state imbalances would be computed for a specific disturbance, we analyze a uniform time delay disturbance between every pair of switches and the pair closest to the input voltage source for the five-level converter. Fig. 13 shows the inductor current in phase #1 because of this disturbance. The shaded area shows the disturbance charge that would result on flying capacitor (1,1). As with Section IV-B, we compute the disturbance charge on every capacitor (a total of six). At steady-state, eq. (19) yields the steady-state flying capacitor voltage imbalances

$$\tilde{\mathbf{v}}_{fly} = \begin{bmatrix} \tilde{v}_{fly}^{(1,1)} \\ \tilde{v}_{fly}^{(2,1)} \\ \tilde{v}_{fly}^{(2,2)} \\ \tilde{v}_{fly}^{(2,2)} \\ \tilde{v}_{fly}^{(1,3)} \\ \tilde{v}_{fly}^{(2,3)} \end{bmatrix} = -\mathbf{A}^{-1} \mathbf{Q}_{dist} \approx V_{dc} \times \frac{\Delta t}{T} \begin{bmatrix} 3 \\ -3 \\ 2 \\ -2 \\ 1 \\ -1 \end{bmatrix}, \quad (31)$$

if we take the coupled inductors as tightly coupled with $L_{\rm cross} = L_{\rm same}$. Again, the flying capacitor imbalances have magnitudes and signs determined by the switching order. Like in the M-phase case, the imbalance depends on the relative severity of the time delay compared to the period.

D. Balancing with Partially Coupled Inductors

So far, we have assumed the inductors are fully coupled and that the converter losses are negligible. In this section, we show that tightly coupled inductors minimize the imbalance and illustrate the effect that losses and natural balancing have in conjunction with coupled inductor balancing.

In a practical circuit with losses, natural balancing and coupled inductor balancing act simultaneously, and the combination of the balancing effects determines the steady-state flying capacitor voltages. If the inductors are uncoupled, there is only natural balancing. If the inductors are very tightly coupled, natural balancing is overshadowed by the much stronger coupled inductor balancing effect. In terms of the feedback diagrams in Section III, coupled inductor and natural balancing are two parallel feedback paths, and the stronger path will exert the most prominent balancing effect.

Fig. 14 illustrates how the strength of coupled inductor balancing increases as the coupling ratio $\frac{L_{\mu}}{L_{l}}$ is increased. As the coupling ratio increases, coupled inductor balancing becomes stronger. Natural balancing, meanwhile, has constant strength since the losses remain the same. For very loose or no coupling, natural balancing dominates. As coupling increases, coupled inductor balancing overtakes natural balancing and reaches a much higher total balancing strength, which leads to smaller voltage imbalances at steady-state. When the coupling ratio becomes very high, the balancing strength reaches the limits derived in sections IV-B and IV-C, where we assumed fully coupled inductors.

Case Study: Partially Coupled Four-Phase Converter

In this case study, we simulate the flying capacitor imbalances of a four-phase converter as we vary the inductors from being uncoupled to very tightly coupled. Fig. 15 shows the simulation results of a four-phase, three-level FCML converter with a $\Delta t=2$ ns delay as the disturbance, $f_{sw}=500$ kHz, $C_{\rm fly}=1~\mu{\rm F},\,L_l=300$ nH and d=0.125 as a function of the coupling ratio $\frac{L_\mu}{L_l}$. At very low coupling ratios, the inductors are almost uncoupled and the flying capacitor voltages are determined primarily by natural balancing. As the coupling ratio increases, the strength of coupled inductor balancing increases, which causes the flying capacitor imbalances to decrease. In fact, the imbalance voltages decrease within the envelope outlined by the dotted lines from the predicted

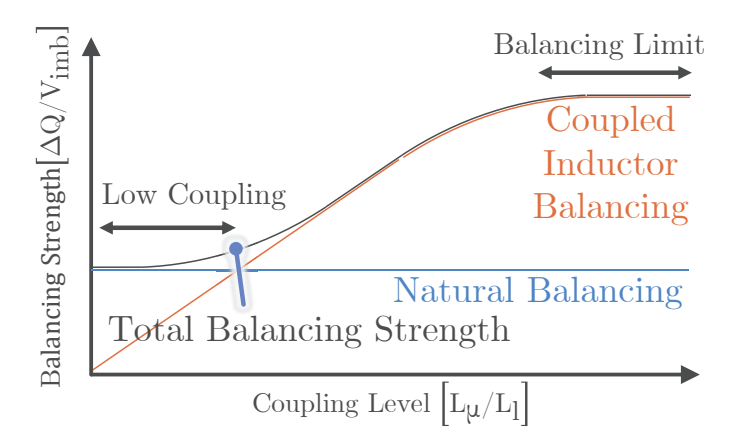


Fig. 14. Combination of natural and coupled inductor balancing. As the coupling level increases, coupled inductor balancing becomes stronger than natural balancing and dominates the balancing characteristics. Very tightly coupled inductors reach the maximum limit of balancing strength.

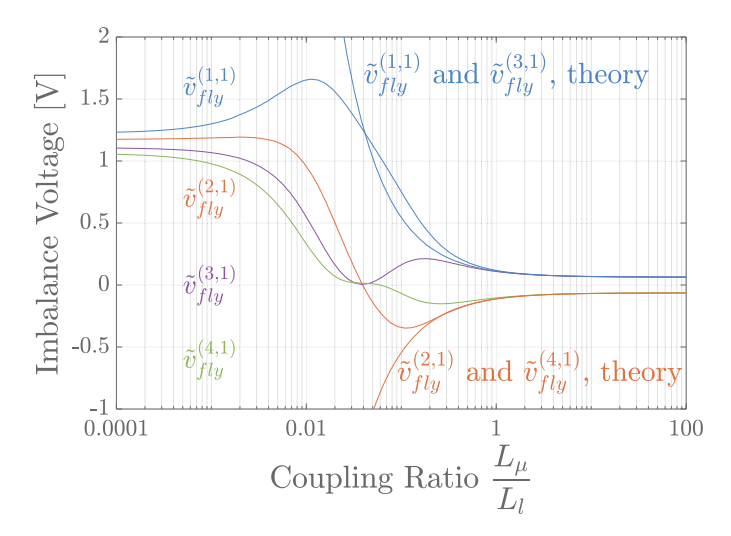


Fig. 15. Simulated flying capacitor voltage imbalances of a four-phase, three-level converter plotted vs. the coupling ratio with $V_{\rm dc}=16$ V, $f_{sw}=500$ kHz, a $\Delta t=2$ ns delay, and d=0.125. As the coupling ratio increases, the strength of coupled inductor balancing increases and reduces the imbalance.

imbalances from Section IV-B. At very high coupling ratios, the flying capacitor imbalances are minimized.

With a low to moderate coupling ratio (L_{μ}/L_{l}) between about 0.01 and 1), the strength of the balancing mechanisms is comparable. This explains how $v_{\rm fly}^{(1,1)}$ initially increases under the influence of multiple balancing factors which lead it to compensate for the other phases with a high imbalance. Since this could negatively impact one of the phases even though the others are improved, it is advisable to have a high coupling ratio such that coupled inductor balancing dominates natural balancing. This minimum depends on the application, but Fig. 15 shows that even a modest coupling ratio of $\frac{L_{\mu}}{L_{l}}=1$ yields most of the balancing benefits.

V. SINGULARITIES WHERE COUPLED INDUCTOR BALANCING FAILS

Section IV derives a mathematical framework that proves the balancing capabilities of coupled inductors. The only

TABLE II Number of Singularities in Multiphase Three-level FCML Converter Balancing Matrix for $0 < d \leq 0.5$, with symmetry for the 0.5 < d < 1 range

	Duty cycle regime i									
IVI	1	2	3	4	5	6	7	8	9	10
2	0	0								
4	0	0	2	0						
6	0	0	1	1	0	0				
8	0	0	2	0	0	0	4	0		
10	0	0	2	1	0	0	0	1	0	0

theoretical limitations found so far are the requirement of an even number of phases, a moderate coupling ratio, and the fact that balancing may become weaker as the number of flying capacitors increases. However, these derivations assume perfectly coupled inductors and only certain duty cycle regimes. In this section, we consider all operating conditions and prove that coupled inductors balance FCML converters for almost all duty cycles and coupling ratios. In doing so, we also find point singularities where coupled inductor balancing fails if there are more than two phases or three levels. We predict the location of these singularities and show how they place theoretical limits on the number of balanced phases, levels, and the required coupling ratio.

A. Duty Cycle Singularities with More Than Two Phases

While coupled inductors can balance any even number of three-level phases for $d < \frac{1}{2M}$ as shown in Section IV-B, we must also treat the other duty cycle regions. The procedure for determining the balancing capability in any duty cycle region is similar to the approach in Section IV: i) compute the balancing matrix, ii) compute the determinant, and iii) find the conditions, if any, for which the determinant is zero.

In Appendix V, we note that if the phase converter operation is symmetric and every phase has the same phase shift, the balancing matrix is skew-symmetric. This property can be used to show that **coupled inductor balancing almost always** works for any even number of phases, any number of levels, and any duty cycle:

$$|\mathbf{A}| \neq 0 \quad \forall \quad d \in (0,1), d \notin \mathcal{D}.$$
 (32)

Equation (32) asserts that the balancing matrix has nonzero determinant and the converter is balanced for all cases except for a finite set of duty cycle singularities \mathcal{D} with size $n(\mathcal{D}) \leq M^2K(K+1)$.

This analysis reveals that coupled inductor balancing fails at specific duty cycles depending on the number of phases and levels. These singularities exist because the elements of the balancing matrix are functions of the d and there are some values of d for which the balancing matrix is singular. We can find these values by solving for the roots of the determinant. Table II lists the number of singularities for three-level converters and the duty cycle regime i they occur in, where the duty cycle is $\frac{i-1}{M(K+1)} < d \leq \frac{i}{M(K+1)}$. There are no singularities for the two-phase converter, but the number of singularities increases as the number of phases increases,

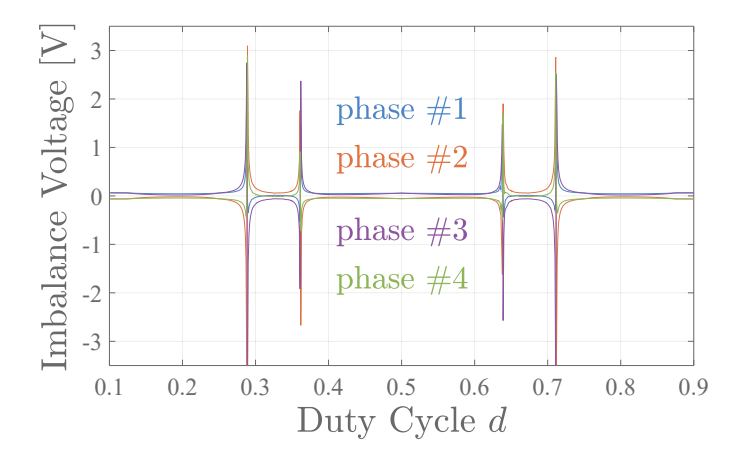


Fig. 16. Simulated flying capacitor voltage imbalances of a four-phase converter with $V_{\rm dc}=16$ V, $f_{sw}=500$ kHz, and a time delay disturbance of $\Delta t=2$ ns on each phase. There are singularities in the balancing matrix at certain duty cycles, resulting in diverging capacitor voltages.

putting a theoretical limitation on the number of phases and levels that can be balanced.

Using multiple two-phase coupled inductors instead of a single multiphase coupled inductor can improve balancing performance. This is because there are no duty cycle singularities with two-phase coupled inductors, as proven in this section, combined with the analysis in section IV-B and equations (25) and (28) showing that the balancing strength decreases with increasing phases. Using multiple two-phase coupled inductors may lead to higher ripple or larger size compared to one multiphase coupled inductor. [24].

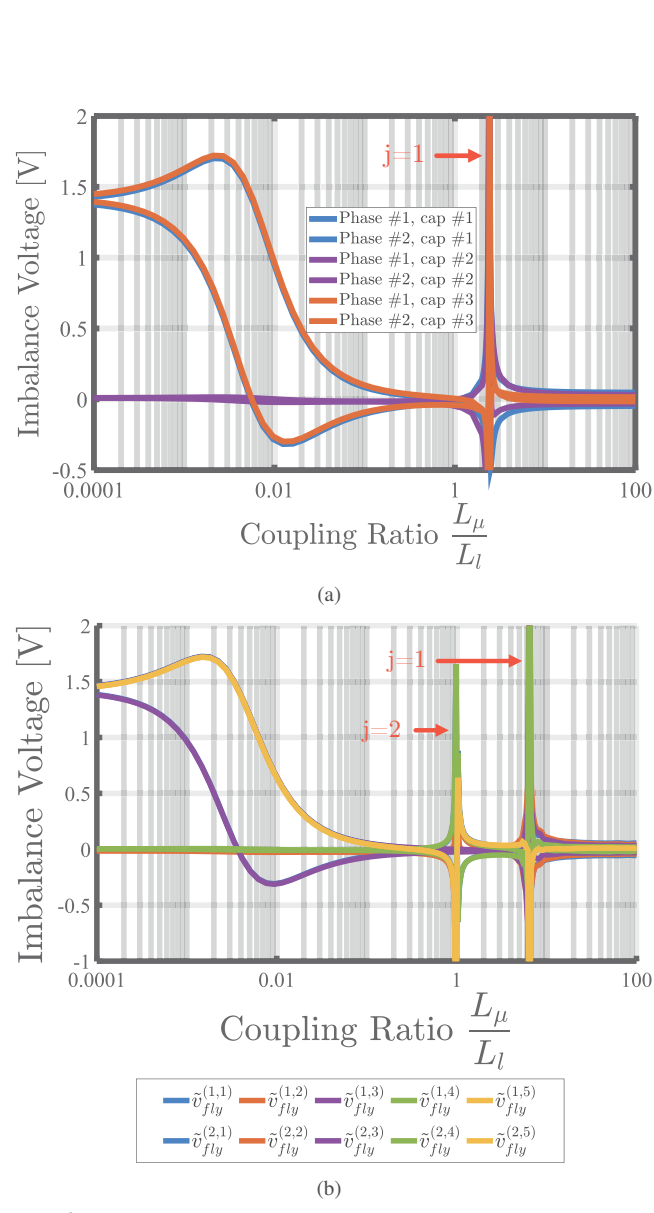
Case Study: Four-phase Converter Singularities

We now consider a numerical example to illustrate the impact of the duty cycle singularities. In Appendix V, we derive the balancing matrix of the four-phase, three-level converter and numerically compute the duty cycles at which the balancing matrix is singular, finding two such duty cycles at $\mathcal{D} = \{0.2836, 0.3629\}$, which are both in the $\frac{1}{4} < d \le \frac{3}{8}$ region. Theoretically, coupled inductor voltage balancing is not effective at these two duty cycles. Fig. 16 shows the simulated imbalances with a $\Delta t = 2$ ns delay, $f_{sw} = 500$ kHz, $C_{\rm fly}=1~\mu{\rm F}$, and $L_{\mu}/L_{l}=100$. The coupled inductors balance the four flying capacitor voltages for most duty cycles, but divergence can be observed at the predicted duty cycle points, along with their mirrored counterparts across the d = 0.5 axis. In a practical converter, there are asymmetries, losses, and nonidealities that could reduce the divergence at the singularity points.

B. Coupling Ratio Singularities with More Than Three Levels

In Section IV-C and IV-D, we showed that fully coupled inductors can balance FCML converters with any finite number of levels, and that the balancing strength tends to improve as the coupling ratio is increased. We now treat partially coupled inductors and find that balancing works for almost all coupling ratios except at specific coupling singularities.

To find the coupling singularities, we use the same procedure of computing the balancing matrix and finding



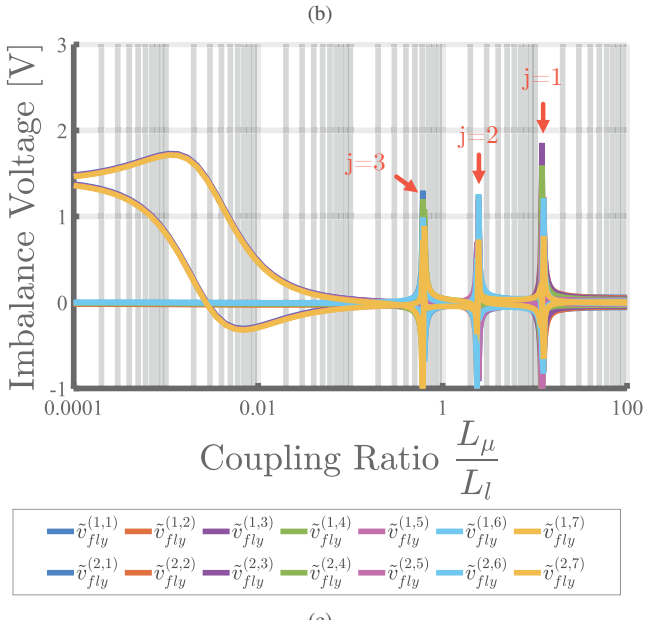


Fig. 17. Simulated flying capacitor imbalance voltages of a two-phase FCML converter with (a) five, (b) seven, or (c) nine levels. The simulations use $V_{\rm dc}=16$ V, $\Delta t=2$ ns, $f_{sw}=500$ kHz, $L_l=300$ nH and $d=\frac{1}{2(K+1)}$. As the number of levels increases, the number of coupling ratio singularities in the balancing matrix, annotated by index j from eq. (33), increases.

TABLE III
CIRCUIT PARAMETERS OF THE FCML PROTOTYPE

Parameter/Component	Value
f_{sw}	500 kHz
$V_{ m dc}$	16 V
C_{flv}	1206 10 μ F × 4
Custom Coupled Inductor L_l	192 nH
Custom Coupled Inductor L_{μ}	7.44 uH
Off-the-shelf Coupled Inductor	Eaton CL1108-4-50TR-R
Two-phase Coupled Inductor	Coilcraft PA6605-AL
Discrete Inductor	Coilcraft XAR7030-222MEB
Switches	EPC2024
Controller	TMS320F28379D

the conditions where its determinant is zero, except we find roots of the coupling ratio $\frac{L_{\text{same}}}{L_{\text{cross}}}$ instead of the duty cycle. Coupled inductor balancing works for almost all cases except for a finite number of singular coupling ratios. It is not only important to have a high coupling ratio to maximize balancing strength, but also to avoid coupling singularities that can impact the converter's robustness. To illustrate the coupling ratio restrictions, we turn to a case study of two-phase multilevel FCML converters.

Case Study: Coupling Singularities of a Two-Phase Converter Let us consider a two-phase converter with $d=\frac{1}{2(K+1)}$ and partial coupling. In this case study, we treat the duty cycle as fixed and vary the coupling ratio. Fig. 17 shows the simulated imbalances with a varying coupling ratio for five-, seven-, and nine-level converters. The imbalances generally follow the same pattern as in the four-phase case, with reducing imbalance as coupled inductor balancing strengthens, and the even-numbered capacitors tend to stay well-balanced throughout [31], [33]. However, there are point singularities at certain coupling ratios, with more singularities as the number of levels increases.

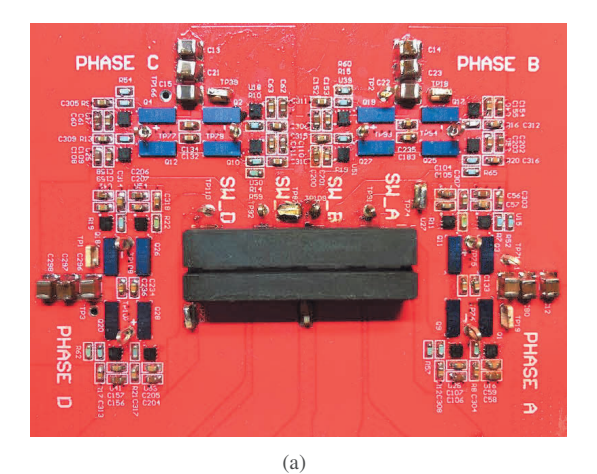
As derived Appendix IV, this case has explicit solutions for the locations of the singularities. If we let the coupling ratio be $x=\frac{L_{\rm same}}{L_{\rm cross}}=\frac{L_{\mu}}{(M-1)L_l+L_{\mu}}=\frac{\mu}{M-1+\mu}$ where $\mu=\frac{L_{\mu}}{L_l}$, the singularities are at

$$x_j = \cos\left(\frac{j}{K+1}\pi\right) \tag{33}$$

for $j=1,\ldots K$. In the simulation, the flying capacitor voltages diverge at exactly these predicted roots; for example, the five-level converter has a predicted root at $x_1=\frac{1}{\sqrt{2}}$, which corresponds to a coupling ratio of approximately $\frac{L_\mu}{L_l}\approx 2.41$. Eq. (33) also shows that the number of coupling singularities increases as the number of levels increases. The largest singularity, which occurs at j=1, approaches $x_1\to 1$ as $K\to\infty$. As the number of levels increases, the required coupling ratio also increases.

VI. EXPERIMENTAL VERIFICATION

The theoretical predictions are verified using FCML converters with two or four phases and between three and five levels. Fig. 18 shows the two-phase, five-level and four-phase, three-level boards. The prototypes have the component values



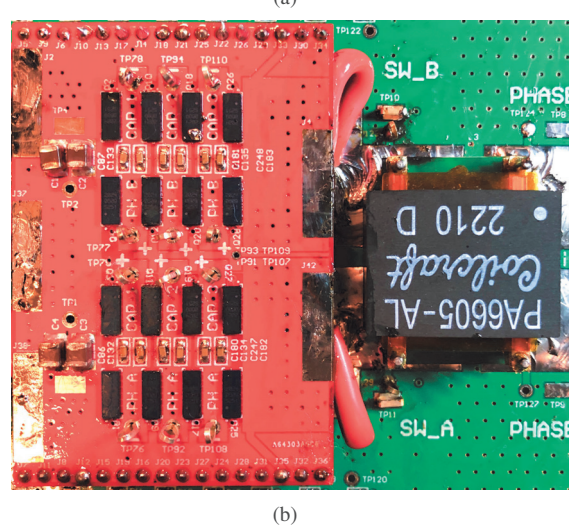
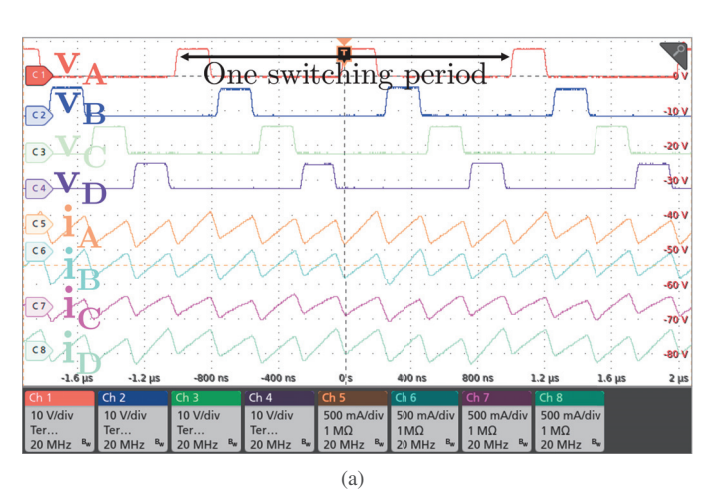


Fig. 18. (a) A four-phase, three-level FCML converter with off-the-shelf Eaton four-phase coupled inductor and (b) a two-phase, five-level FCML converter with off-the-shelf Coilcraft PA6605-AL inductor.

shown in Table III, with the five-level converter having a lower switching frequency of 50 kHz due to gate driving limitations. To compare coupled inductor balancing to natural balancing, four inductors are used: discrete 2.2 $\mu{\rm H}$ inductors, an off-the shelf Eaton CL1108-4-50TR-R four-phase coupled inductor with $\frac{L_{\mu}}{L_{l}}=2.66$, a custom four-phase coupled inductor with $\frac{L_{\mu}}{L_{l}}=38.9$, and an off-the-shelf Coilcraft PA6605-AL two-phase coupled inductor with $\frac{L_{\mu}}{L_{l}}=38.5$, which all have sufficient steady-state inductance for low ripple. The flying capacitors are rated for 50 V and have a class II X8L dielectric. The capacitances are selected to have small voltage ripple with the given load and switching frequency. At the selected input voltage, the capacitance varies around 10% for different dc biases in the five-level converter. If a higher input voltage is used, the effect of dc bias on different flying capacitors should be considered in a higher order converter.

The operating waveforms of the four-phase converter at d=0.1 are shown in Fig. 19 with the (a) tightly coupled $\left(\frac{L_{\mu}}{L_{l}}=38.9\right)$ inductors and (b) discrete inductors. Due to the three-level FCML structure and interleaving with coupled inductors, the effective ripple frequency is multiplied by eight. This considerably reduces the ripple amplitude.



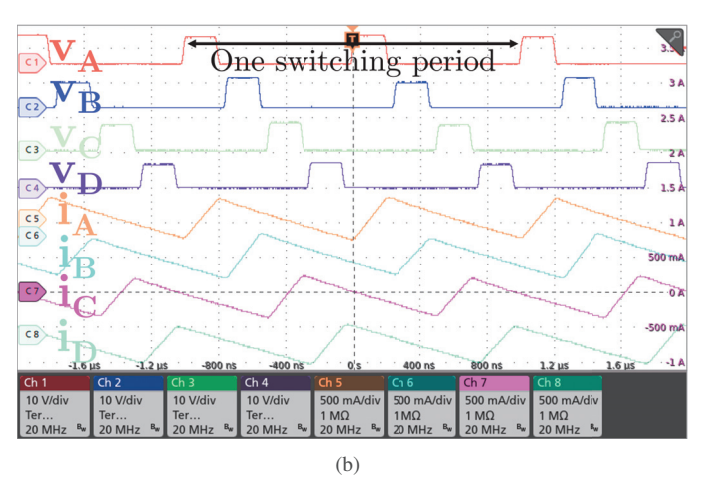


Fig. 19. Measured switching waveforms of four-phase, three-level FCML converter with (a) coupled inductors and (b) discrete inductors. Because of the coupled inductors, the ripple frequency is four times higher with coupled inductors than discrete inductors.

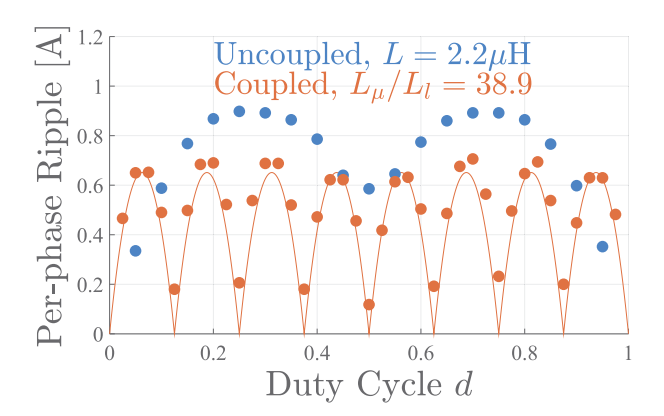


Fig. 20. Measured per-phase current ripple average of the four phases. The inductors are chosen to have similar maximum ripple. Despite this, the coupled inductors generally have significantly lower ripple due to additional ripple cancellation points, matching well with the theoretical ripple shown by the dotted line. The uncoupled inductor ripple does not cancel at d=0.5 due to flying capacitor voltage imbalances, even with no disturbances.

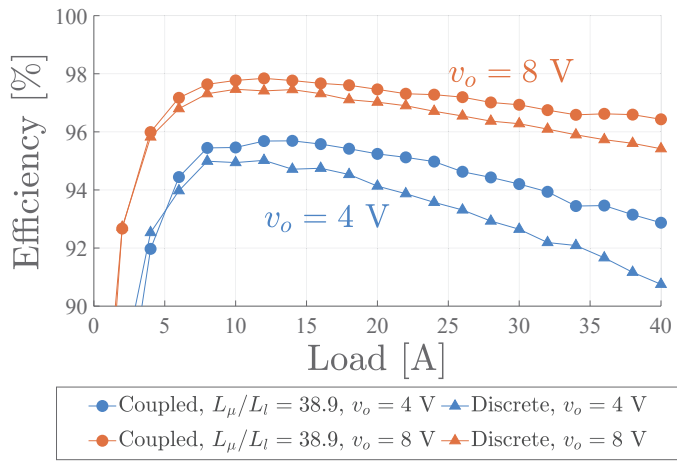


Fig. 21. Measured converter efficiency at $v_o=8~{\rm V}$ and $v_o=4~{\rm V}$, demonstrating coupled inductor efficiency improvements.

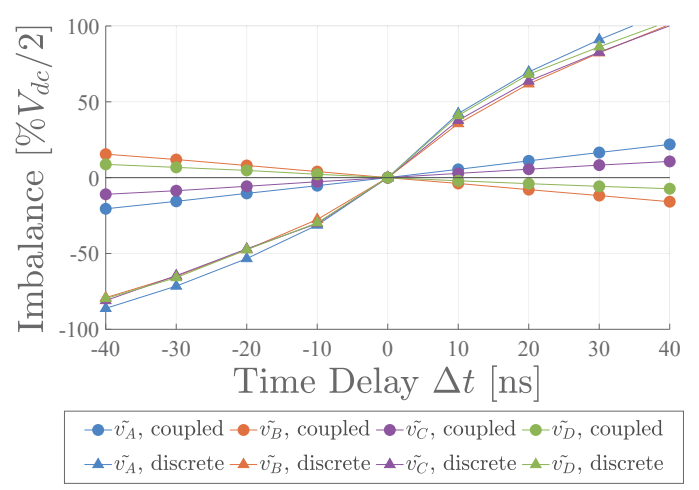


Fig. 22. Flying capacitor voltage imbalance as a function of the time delay Δt at d=0.125. With coupled inductors, the imbalance scales linearly with Δt , as predicted in eq. (25), and are much smaller with coupled inductors.

The inductors compared in these experiments are selected to have similar ripple, as shown in Fig. 20. Because of this, the coupled inductors have a much lower leakage inductance of $L_l=192$ nH compared to the discrete inductance of 2.2 μ H. Therefore, the coupled inductor converter will have a much faster transient response, allowing it to respond to load transients more effectively [23]. Despite this, the coupled inductor converter still has lower ripple due to ripple cancellation at more duty cycles. Fig. 21 shows the converter efficiency being improved by coupled inductors.

To verify the balancing performance, a time delay of one set of switches between -40 ns and +40 ns is introduced using the digital controller. Fig. 22 shows the measured flying capacitor voltage imbalances of the four-phase, three-level converter at d=0.125 as a function of the delay magnitude. The coupled inductors balance the flying capacitors much better than natural balancing, which reduces the voltage stress, ripple, and distortion.

Coupled inductor balancing improves as the coupling ratio increases, as shown in Fig. 23. In these plots, the imbalance

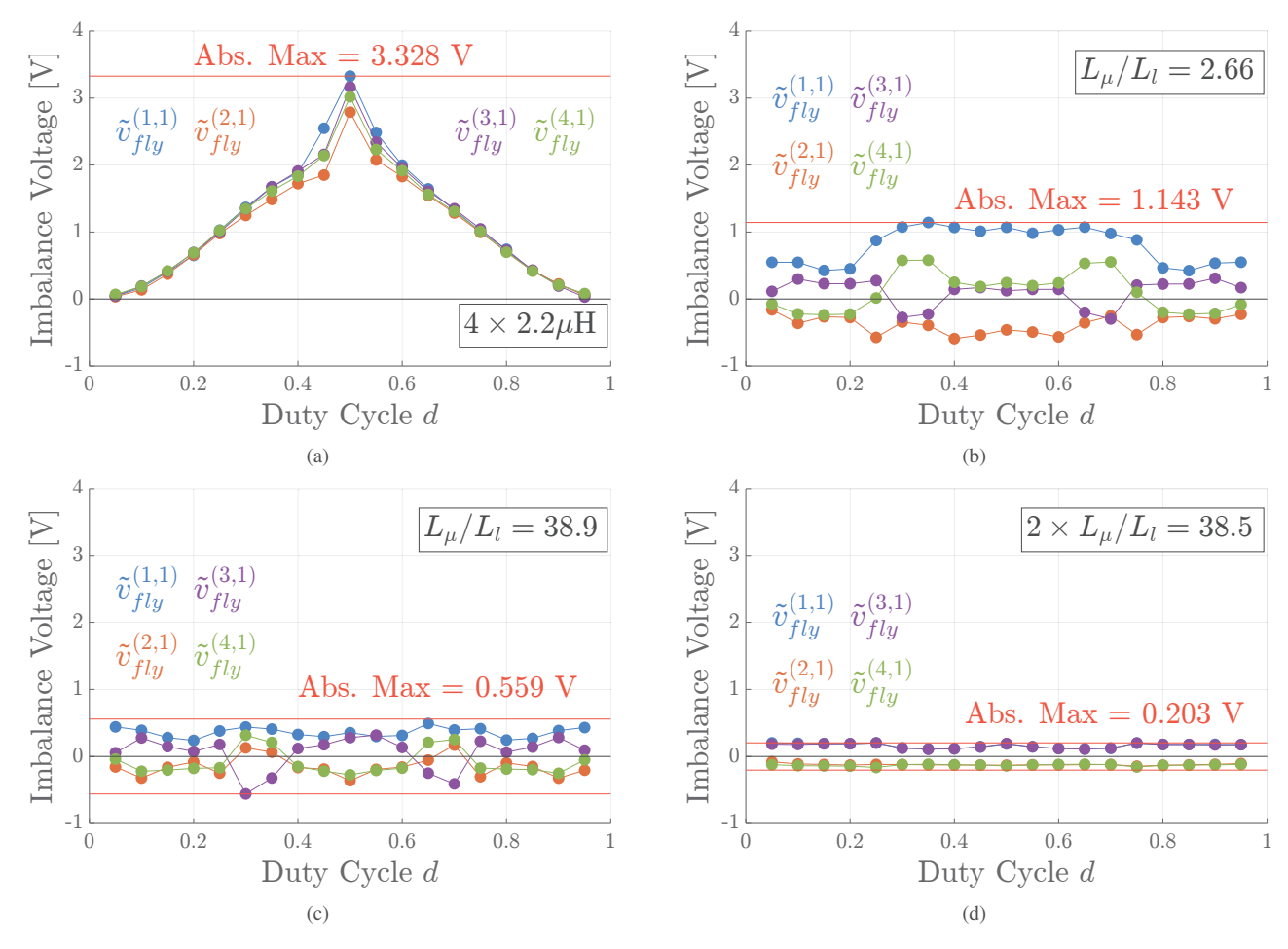


Fig. 23. Flying capacitor voltage imbalances with constant time delay $\Delta t=10$ ns and (a) four discrete 2.2 μ H inductors, (b) off-the-shelf four-phase coupled inductors with $\frac{L_{\mu}}{L_{l}}=2.66$, (c) custom four-phase coupled inductors with $\frac{L_{\mu}}{L_{l}}=38.9$, and a pair of two-phase coupled inductors with $\frac{L_{\mu}}{L_{l}}=38.5$. The input voltage is $V_{\rm dc}=16$ V.

is plotted across the duty cycle range for a time delay of $\Delta t=10$ ns. With uncoupled inductors (a), the imbalances are large and reach an absolute maximum of 3.328 V. With the tightly coupled custom inductors (c), the imbalance is consistently limited to 0.559 V across the duty cycle range. With the off-the-shelf coupled inductors (b), which have a coupling ratio between the other two of $\frac{L_{\mu}}{L_{l}}=2.66$, the balancing is less effective. The absolute maximum imbalance is 1.143 V, which is still considerably reduced compared to the results with discrete inductors.

As shown in Section IV-B, coupled inductor balancing becomes weaker and less reliable as the number of coupled inductor phases increases. However, these experiments show that a single four-phase coupled inductor is still suitable for balancing a four-phase converter. It is also possible to use two two-phase coupled inductors instead, which is the most reliable configuration. Fig. 23(d) shows the imbalances with two two-phase coupled inductors with $\frac{L_{\mu}}{L_{l}}=38.5$ coupling phase #1 with phase #2 and phase #3 with phase #4.

Fig. 24 shows the measured imbalances of a fourphase, three-level converter where one complimentary pair of switches is phase shifted by 8° from ideal. The capacitor voltages are generally kept well balanced but do spike at four duty cycle points. These spikes coincide exactly with the singularities for a four-phase converter predicted in Section V to occur at $\mathcal{D}=\{0.2836,0.3629\}$ and the corresponding points across the d=0.5 axis. This experiment verifies both the existence of multiphase singularities and the validity of the balancing matrix approach for predicting their locations.

Fig. 25 shows the measured voltage imbalances of a two-phase, five-level converter with a time delay of $\Delta t=300$ ns applied to each phase. A larger time delay is used to emphasize the imbalance since the switching period is longer. The coupled inductors keep the flying capacitors balanced for most duty cycles, but they diverge at d=0.5. This is a nominal conversion ratio where the five-level converter is intrinsically imbalanced and another balancing mechanism is needed.

Fig. 26 verifies the balancing performance across load. Coupled inductor balancing maintains similar balancing performance at both high and low loads, making it applicable to a variety of operating conditions. Fig. 27 verifies that coupled inductor balancing functions well for a variety of randomized phase shift disturbances, both positive and negative, on all switches. A random phase shift between $\pm 7^{\circ}$, equivalent to ± 40 ns, is applied to all of the switches on the four-phase, four-level converter. Very large disturbance magnitudes are

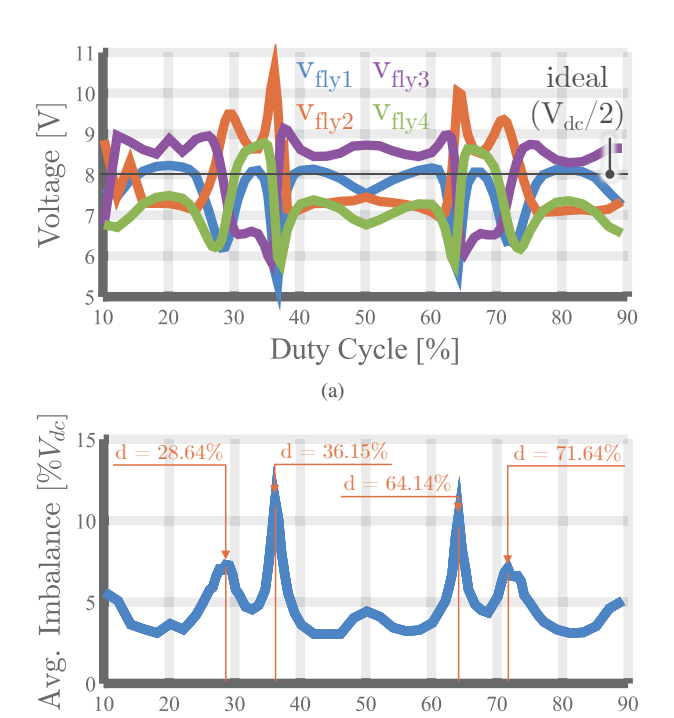


Fig. 24. (a) Flying capacitor voltages of the four-phase converter kept well-balanced with a 8° phase shift on one complimentary pair of switches and a 6 A load. (b) Singularities of the four-phase converter at the theoretically predicted duty cycles.

(b)

Duty Cycle [%]

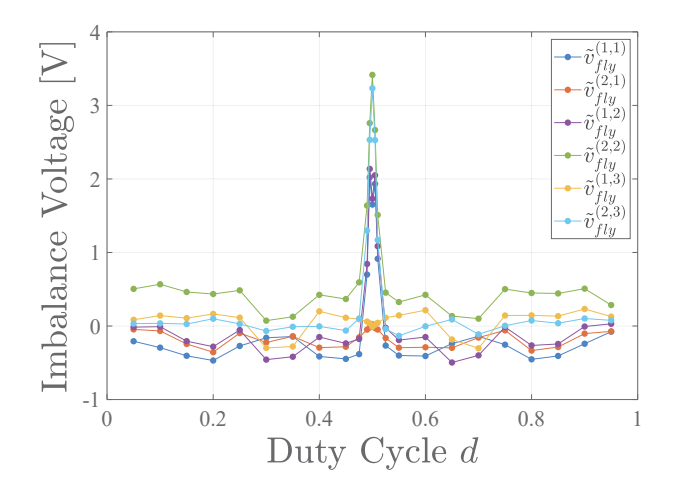


Fig. 25. Flying capacitor voltage imbalances of two-phase, five-level converter with $V_{\rm dc}=16~{\rm V}$ and time delay $\Delta t=300$ ns unbalancing the flying capacitors.

used to emphasize the imbalance. In a practical circuit, the disturbances would likely be smaller.

VII. COMPARISON WITH OTHER BALANCING TECHNIQUES AND DESIGN GUIDELINES

Having explained the fundamental mechanism of coupled inductor balancing, we can now compare its strengths and weaknesses to other common balancing techniques. Table IV compares the impact of each method on voltage balancing, size, current ripple, loss, and complexity. Although converters

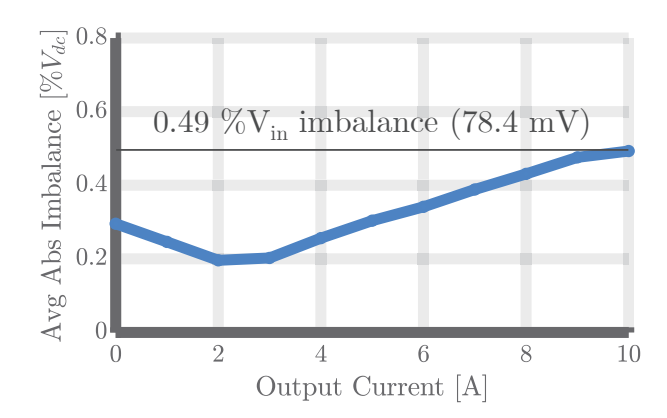


Fig. 26. Average absolute flying capacitor voltage imbalance for four-phase, four-level FCML converter across output load at d=0.25 and $V_{\rm dc}=16$ V.

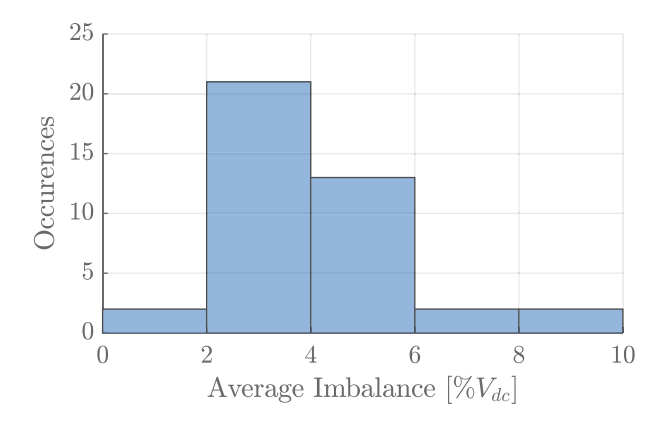


Fig. 27. Histogram of average absolute imbalances with random phase shift disturbances on all switches between $\pm 7^\circ \equiv 40$ ns at $f_{sw}=490$ kHz and a 5 A load.

with an even number of levels are less sensitive [33], natural balancing [12] has the general drawback of variability and dependence on losses, and is not typically relied on as a sole balancing method. Active balancing [35] uses measurement or estimation of the flying capacitor voltages and active control to balance them. This is a very flexible and robust technique that can handle many unbalanced structures. Additionally, active balancing can, with appropriate feedback control, force the steady-state imbalance to be zero, while passive balancing methods like coupled inductors will still have a nonzero, albeit small, remaining imbalance. However, it does have the disadvantage of needing additional hardware and control for every flying capacitor that must be balanced, and the control bandwidth is limited. Additionally, some active balancing techniques rely on the load current to balance the capacitors and do not work at light load, while coupled inductor balancing works independently of the load current.

Compared to other existing balancing approaches, coupled inductor balancing offers the following advantages: i) Strong voltage balancing without the need to rely on converter losses or complex sensing and control hardware, ii) Good scaling to higher-order multilevel multiphase converters where more capacitors must be balanced, or high bandwidth applications with high switching frequencies; iii) Can be combined with using an even number of levels or other balancing approaches

	Coupled Inductor	Natural Balancing	Active Balancing	Even-level Switching
References	[1]–[3], [42]	[9]–[12]	[32], [35]	[30], [31]
Balancing Strength	Strong	Weak	Strong	Depends
Steady-State	Yes	Yes	Yes	Partially
Transient	Faster	No change	Depends	No change
Reliant on Losses	No	Yes	No	No
Applicability	Even # phases, any # levels	Any # levels	Any # levels	Even # levels
Inductor Size	Reduced	No change	No change	No change
Current Ripple	Reduced	No change	No change	No change
Load Dependence	No	Yes	Sometimes	No
Passivity	Passive	Passive	Active	Passive

TABLE IV
COMPARISON OF FCML VOLTAGE BALANCING TECHNIQUES

to provide good balancing in all cases; iv) Acceleration of the dynamic voltage balancing and transient response by reducing transient inductance; v) Inherent ripple reduction that can improve efficiency, switch stress, and saturation flux requirements, all with a smaller size than multiple discrete inductors.

We now summarize general design guidelines for robust flying capacitor voltage balancing using coupled inductors. Ripple reduction is a primary function of coupled inductor and multilevel converter design. The design guidelines for this purpose have been explored in detail [14], [22], [24], [42]–[45]. In general, the ripple can be reduced by interleaving, increasing the number of phases, increasing the number of levels, and designing tightly coupled inductors.

To minimize capacitor voltage imbalances in FCML converters using coupled inductors, the following guidelines are recommended for selecting the number of phases, flying capacitor levels, and coupling coefficients:

- Use an even number of phases: coupled inductor balancing works for an even number of phases and is not effective for an odd number of phases.
- Avoid using very high number of phases: the balancing mechanism gets weaker as the number of phases increases.
- 3) Use an even number of levels: while coupled inductor balancing works for any finite number of levels, an even number of levels aids capacitor voltage balancing in coupled and uncoupled FCML converters alike, especially at nominal conversion ratios.
- 4) **Maximize the coupling coefficient**: maximizing the coupling coefficient minimizes the imbalance and offers the most ripple reduction for a given transient response.

VIII. CONCLUSION

This paper proves that coupled inductors are effective at balancing flying capacitor voltages in multiphase FCML converters. The voltage balancing capabilities are derived for an arbitrary multiphase converter, and it is shown that any even number of phases may be balanced for most duty cycles, and the magnitude of the steady-state imbalances may be predicted theoretically. Multiphase converters with more than two phases are shown to have singularities at certain duty cycles where balancing fails, though these may be suppressed

in practical designs. With other conditions held constant, twophase coupled inductors are shown to minimize the imbalance without susceptibility to singularities that higher-order coupled inductors have. Coupled inductors are shown to balance FCML converters with any number of levels if the coupling ratio is high enough, and may be used to balance any number of flying capacitors so long as there are an even number of phases. Partially coupled inductors will also balance the flying capacitors in some cases, though some coupling ratios will result in divergence. Coupled inductor balancing is shown to apply to a variety of disturbances and to intrinsically unbalanced FCML structures. The theoretical results are experimentally verified with a four-phase, three-level FCML converter, a four-phase, four-level FCML converter, and a two-phase, five-level FCML converter. Design guidelines for the number of phases, number of levels, and coupling coefficient for robust FCML converters are recommended.

ACKNOWLEDGEMENTS

This work was supported by the National Science Foundation (Award #1847365) and the Natural Sciences and Engineering Research Council of Canada (Award #557270 – 2021).

APPENDIX I EXPANDED MODELS FOR COUPLED INDUCTORS

A multiphase coupled inductor integrates multiple windings on a single magnetic core. Fig. 28 shows an example four-phase coupled inductor. Assuming the core is symmetric and the top and bottom plates have negligible reluctances, the voltages and currents in the inductor can be described using the inductance dual model [24] as

$$N^{2} \begin{bmatrix} \frac{di_{1}}{dt} \\ \frac{di_{2}}{dt} \\ \vdots \\ \frac{di_{M}}{dt} \end{bmatrix} = \begin{bmatrix} \mathcal{R}_{L} + \mathcal{R}_{C} & \mathcal{R}_{C} & \cdots & \mathcal{R}_{C} \\ \mathcal{R}_{C} & \mathcal{R}_{L} + \mathcal{R}_{C} & \cdots & \mathcal{R}_{C} \\ \vdots & \vdots & \ddots & \vdots \\ \mathcal{R}_{C} & \mathcal{R}_{C} & \cdots & \mathcal{R}_{L} + \mathcal{R}_{C} \end{bmatrix} \begin{bmatrix} v_{1} \\ v_{2} \\ \vdots \\ v_{M} \end{bmatrix}.$$
(34)

Here, i and v are the current through and voltage over each of the M windings. Each winding has N turns and \mathcal{R}_L and \mathcal{R}_C are the side leg and center leg reluctances respectively, as indicated in Fig. 28. As the center leg reluctance increases or the side leg reluctance decreases, the inductor becomes more coupled. Higher coupling reduces ripple and transient inductance, and also improves voltage balancing capability.

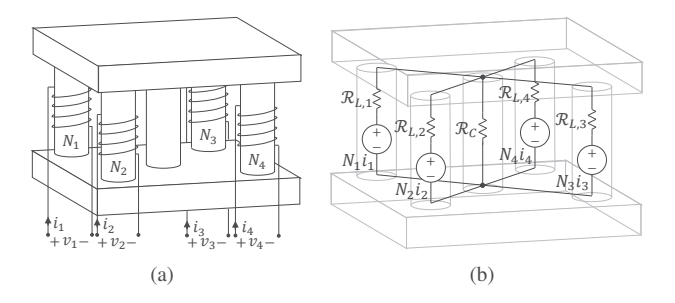


Fig. 28. (a) Drawing of a symmetric four-phase coupled inductor, and (b) reluctance model of a four-phase coupled inductor with center leg reluctance \mathcal{R}_C and side leg reluctances $\mathcal{R}_{L,1}\cdots\mathcal{R}_{L,4}$. The reluctances of the top and bottom plates are neglected in the theoretical analysis. They are not required to be negligible in practical designs.

Previous works have detailed optimal coupled inductor design in terms of structure [46], loss [20], integration [22], and transient response [23], [24]. Alternatively, we can parameterize the coupled inductor in terms of its leakage inductance L_l and magnetizing inductance L_{μ} ,

$$L_l = \frac{N^2}{\mathcal{R}_L + M\mathcal{R}_C},\tag{35}$$

$$L_{l} = \frac{N^{2}}{\mathcal{R}_{L} + M\mathcal{R}_{C}},$$

$$L_{\mu} = \frac{N^{2}(M-1)\mathcal{R}_{C}}{\mathcal{R}_{L}(\mathcal{R}_{L} + M\mathcal{R}_{C})}.$$
(35)

 L_l determines the transient performance of a coupled inductor converter [23]. As L_{μ}/L_{t} increases, the inductors become more tightly coupled.

APPENDIX II WAVEFORM STITCHING TECHNIQUE

As a hybrid switched capacitor system, balancing analysis of FCML converters often involves calculating the inductor current over a switching period with many switching states, each with a different duration and circuit state. Therefore, we compute the solution of each switching state separately and "stitch" them together computationally [29].

A. Naturally Balanced FCML Converters

An unbalanced three-level FCML converter has typical switching waveforms shown in Fig. 6. There are four switching sub-periods. First, the flying capacitor is connected through $V_{\rm dc}$ to the switch node and it is charged by the inductor current. Second, the switch node is grounded. Third, the flying capacitor is connected through ground to the switch node and it is discharged by the inductor current. Finally, the switch node is grounded again. These switching states are illustrated in Fig. 29. In this analysis, we assume the duty ratio is smaller than 1/2. Similar analysis can be conducted for other duty ratios with similar results.

In Fig. 6, the flying capacitor is assumed to have a positive imbalance, that is, $v_{\rm fly} > \frac{V_{\rm dc}}{2}$. Therefore, the switch node has unequal pulse amplitudes. The imbalanced component of the switch node is labelled as $\tilde{v}_{\rm sw}$. Our goal is to calculate the inductor current induced by this imbalance using the waveform stitching technique and compute the balancing effect and loss.

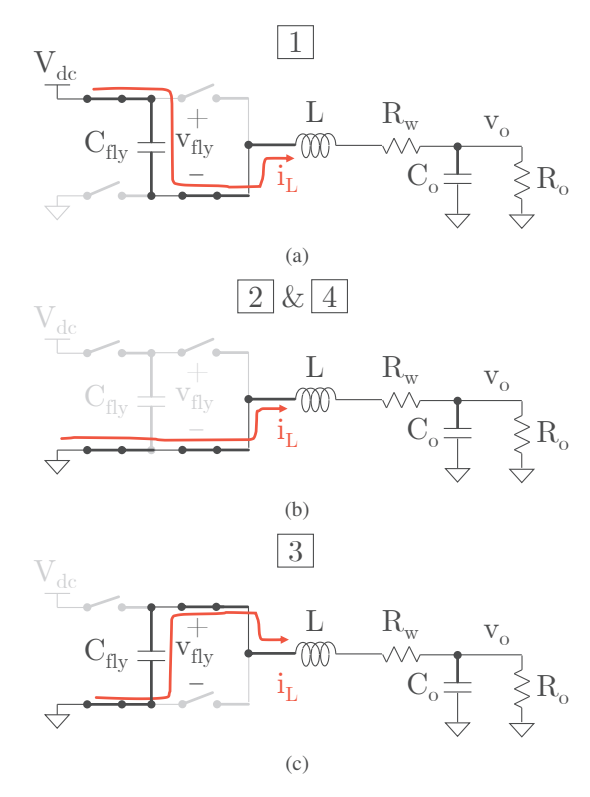


Fig. 29. Equivalent sub-period circuits for the three-level FCML converter.

The imbalanced component of the switch node voltage induces an imbalanced component in the inductor current labelled \tilde{i}_L and is shown for the cases when the winding resistance R_w is zero and nonzero. When the winding resistance is zero, the inductor current ramps linearly and it is obvious that the net charge transfer in the flying capacitor (the shaded areas) is zero. When the winding resistance is nonzero, the inductor current waveform changes exponentially instead of linearly, which is exaggerated in Fig. 6 for effect. The flying capacitor is connected in alternating directions and so it sees a negative average current i_{flv} in both sub-periods #1 and #3.

To quantify the charge transferred into the flying capacitor, we compute the inductor current. We first write the current in each sub-period as a function of the current at the end of the previous sub-period, then solve for the inductor current in each of the sub-period circuits shown in Fig. 29 as

$$\tilde{i}_{L}^{\#1}(t) = \tilde{i}_{L}^{\#4}(d^{*}T)e^{-\frac{R_{w}}{L}t} - \frac{\tilde{v}_{fly}}{R_{w}}\left(1 - e^{-\frac{R_{w}}{L}t}\right), \quad (37)$$

$$\tilde{i}_L^{\#2}(t) = \tilde{i}_L^{\#1}(dT)e^{-\frac{R_w}{L}t},$$
(38)

$$\tilde{i}_{L}^{\#3}(t) = \tilde{i}_{L}^{\#2}(d^{*}T)e^{-\frac{R_{w}}{L}t} + \frac{\tilde{v}_{fly}}{R_{co}}\left(1 - e^{-\frac{R_{w}}{L}t}\right), \quad (39)$$

$$\tilde{i}_L^{\#4}(t) = \tilde{i}_L^{\#3}(dT)e^{-\frac{R_w}{L}t},$$
(40)

where $d^* = \frac{1}{2} - d$. For simplicity, each sub-period current is shifted to start at time t = 0. Each current is simply the current at the end of the previous sub-period (for example, $\tilde{i}_L^{\#1}(dT)$ is the current at the end of sub-period #1 which is used in the equation for sub-period #2), which decays exponentially, plus a possible forcing function. We need one initial condition to fully define the current. This condition comes from our assumption that the flying capacitance is large so $\tilde{v}_{\rm flv}$ does not vary much in a switching period: this means that the average voltage applied to the switch node is zero, and the average inductor current must be zero.

Using the equation of the inductor current with the initial condition applied, we compute the average power loss in the resistor and the charge transferred from the flying capacitor in one period. First, the average power loss in the resistor is

$$\left\langle \tilde{P}_{R_w} \right\rangle = R_w \left\langle \tilde{i_L}^2 \right\rangle$$

$$= \frac{R_w}{T} \int_0^T \tilde{i_L}^2 dt \qquad (41)$$

$$\left\langle \tilde{P}_{R_w} \right\rangle \approx \frac{R_w T^2 d^2 \tilde{v}_{\text{fly}}^2 (3 - 4d)}{12L^2}$$

$$= \frac{\gamma}{R_w Q_L^2} \tilde{v}_{\text{fly}}^2. \qquad (42)$$

Here, the integral of the square inductor current in (41) is calculated symbolically from the inductor current in eq. (37) through (40). In the final result (42), $\gamma = \frac{d^2(3-4d)\pi^2}{3}$ is a scaling factor depending on the duty cycle and $Q_L = \frac{\omega_{\rm sw}L}{R_{\rm in}}$ is the quality factor of the inductor at the switching frequency. The power loss is derived by approximating exponential terms with a third-order Taylor series and assuming the quality factor of the inductor is high [1]. The power loss has the general form of a squared voltage divided by the resistance, where the voltage $\frac{\tilde{v}_{\text{fly}}}{Q_L}$ is approximately the voltage over R_w . The net charge into the flying capacitor during one period

is

$$\Delta Q = \int_0^{dT} \tilde{i}_L^{\#1}(t) dt - \int_0^{dT} \tilde{i}_L^{\#3}(t) dt$$

$$\approx \frac{\gamma T}{R_w Q_L^2} \tilde{v}_{\text{fly}}, \tag{43}$$

since the capacitor is charged in sub-period #1 and discharged in sub-period #3. The average current into the flying capacitor is therefore

$$\frac{\Delta Q}{T} = \frac{\gamma}{R_w Q_L^2} \tilde{v}_{\text{fly}} = \frac{\left\langle \tilde{P}_{R_w} \right\rangle}{\tilde{v}_{\text{fly}}} = \tilde{i}_{\text{bal}}, \tag{44}$$

which is exactly equal to the average power dissipated in the resistor divided by the imbalance voltage, which we define in eq. (10) as the balancing current i_{bal} . Therefore, equations (41) and (44) verify the conclusion in Section III-A that the small-signal power loss induced by the flying capacitor imbalance relates to the effective flying capacitor balancing current.

B. Derivation of Timing Factor for Feedback Model of Coupled Inductor Balancing

The same waveform stitching method can be applied to coupled inductor converters. Since coupled inductor balancing does not rely on any losses, the current waveforms are linear, making the analysis much simpler. As explained in Section III, the imbalance voltage of one phase in a two-phase converter will cause a balancing current in the other phase that tends

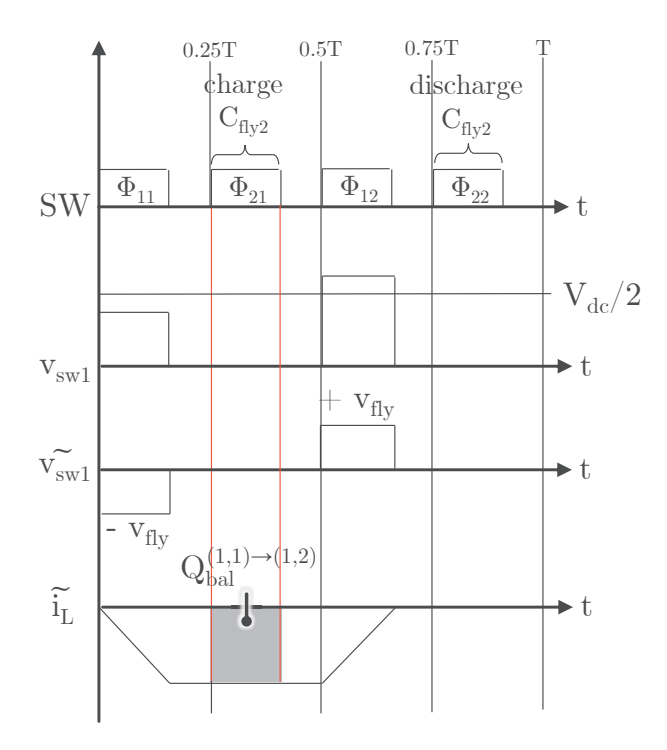


Fig. 30. Switching waveforms of two-phase, three-level FCML converter used to derive the timing factor in the feedback path.

to cancel out disturbances. To mathematically describe this process, we must study the waveforms in detail.

The switching order is important to the balancing behavior. Note that if phase #1 switches "first", that is, connecting to $V_{\rm dc}$ first, then the order of flying capacitors being connected to the switch node is $-\tilde{v}_{\text{fly1}} \rightarrow -\tilde{v}_{\text{fly2}} \rightarrow +\tilde{v}_{\text{fly1}} \rightarrow +\tilde{v}_{\text{fly2}}$, which is not the same should phase #2 be switched "first".

Fig. 30 shows the balancing waveforms of a two-phase, three-level FCML converter for d < 0.25 and phase #1 switching first. We assume that flying capacitor 1 has a positive imbalance voltage. The imbalance voltage of phase #1 induces an imbalance current in phase #2 because of the coupled inductor. During the charging duration of phase #2, which begins at t = 0.25T, flying capacitor 2 is charged by

$$Q_{\text{bal}}^{(1,1)\to(2,1)} = -\frac{(dT)^2 \tilde{v}_{\text{flyl}}}{L_{\text{cross}}}.$$
 (45)

On average, this means that a balancing current of $-\frac{d^2T\tilde{v}_{\mathrm{fly2}}}{I_{\cdot\cdot\cdot\cdot}}$ is applied to phase #2. A positive flying capacitor voltage imbalance in phase #1 will induce a negative balancing current in phase #2 scaled by $\frac{d^2T}{L_{\rm cross}}$, as shown in Fig. 9. On the other hand, a similar derivation shows that a positive imbalance in phase #2 induces a positive current in phase #1, so the timing factor is $-d^2T$ in this case. Since one timing factor is negative and one is positive, a full traversal of the loop indicates it is in negative feedback. In summary, the waveform stitching method can easily find the balancing relationships between each phase. In particular, a timing factor must be found to account for the order of switching, duration of sub-periods, and their subsequent effect on the balancing matrix to describe the balancing behavior.

APPENDIX III

DERIVATION OF COUPLED INDUCTOR BALANCING CAPABILITIES FOR AN ARBITRARY NUMBER OF PHASES

If we restrict the duty cycle to $d < \frac{1}{2M}$, the balancing matrix **A** takes the form in eq. (22). Let **X** be

$$\mathbf{X} = \begin{bmatrix} 0 & 1 & 1 & 1 & \cdots & 1 \\ -1 & 0 & 1 & 1 & \cdots & 1 \\ -1 & -1 & 0 & 1 & \cdots & 1 \\ -1 & -1 & -1 & 0 & \cdots & 1 \\ \vdots & \vdots & \vdots & \vdots & \ddots & \vdots \\ -1 & -1 & -1 & -1 & \cdots & 0 \end{bmatrix}_{M \times M}$$
(46)

which is the balancing matrix \mathbf{A} with shared scaling terms factored out. If \mathbf{X} has a nonzero determinant, $\mathbf{A}_{M\text{-phase}}$ is invertible, a solution to eq. (18) exists, and the coupled inductor will balance the flying capacitors. \mathbf{X} is skew-symmetric, so if M is odd, $|\mathbf{X}|_{M\text{ odd}} = 0$ [47]. The coupled inductors will not balance the flying capacitors if there are an odd number of phases. If M is even, $|\mathbf{X}| = 1$. Therefore, the balancing matrix is always invertible for an even number of phases M and the coupled inductors can balance the flying capacitors.

To estimate how the balancing strength scales with the number of phases, we compute the inverse of ${\bf A}$ if M is even. The inverse of ${\bf X}$ is

$$\mathbf{X}^{-1} = \begin{bmatrix} 0 & -1 & 1 & -1 & \cdots & -1 \\ 1 & 0 & -1 & 1 & \cdots & 1 \\ -1 & 1 & 0 & -1 & \cdots & -1 \\ 1 & -1 & 1 & 0 & \cdots & 1 \\ \vdots & \vdots & \vdots & \vdots & \ddots & \vdots \\ 1 & -1 & 1 & -1 & \cdots & 0 \end{bmatrix}_{M \times M} , \quad (47)$$

and for a given imbalance vector $\mathbf{Q}_{\text{dist}},$ the steady-state voltage imbalances are

$$\tilde{\mathbf{v}}_{fly} = -\mathbf{A}^{-1} \mathbf{Q}_{dist}
= \frac{L_{cross}}{(dT)^2} \mathbf{X}^{-1} \mathbf{Q}_{dist}.$$
(48)

For a time shift disturbance where each phase has a time shift of Δt_m for $m=1,\ldots,M$, the disturbance vector is

$$\mathbf{Q}_{\text{dist}} = dT \times \frac{dV_{\text{dc}}}{L_l} \begin{bmatrix} \Delta t_1 \\ \Delta t_2 \\ \Delta t_3 \\ \vdots \\ \Delta t_M \end{bmatrix}, \tag{49}$$

following from the derivation in the four phase case in Section IV. Assuming each time shift has a maximum magnitude of Δt and is either positive or negative (lag or lead respectively), we can compute the best- and worst- case imbalance depending on the signs of the time shifts. Without loss of generality, we consider the first flying capacitor. If all the time shifts are in the same direction, then the flying capacitor voltage imbalance is

$$\tilde{\mathbf{v}}_{\text{fly}} = \frac{L_{\text{cross}}}{(dT)^2} \mathbf{X}^{-1} \times dT \frac{dV_{\text{dc}}}{L_l} \begin{bmatrix} \Delta t \\ \Delta t \\ \Delta t \\ \vdots \\ \Delta t \end{bmatrix}$$

$$\rightarrow \tilde{v}_{\text{fly}}^{(1,1)} \Big|_{\text{best-case}} = \frac{V_{\text{dc}} \Delta t L_{\text{cross}}}{T L_l}. \tag{50}$$

In the worst case, the direction of the time shifts alternates. In this case, the worst-case imbalance of capacitor #1 is

$$\tilde{\mathbf{v}}_{fly} = \frac{L_{cross}}{(dT)^2} \mathbf{X}^{-1} \times dT \frac{dV_{dc}}{L_l} \begin{bmatrix} +\Delta t \\ -\Delta t \\ +\Delta t \\ \vdots \\ -\Delta t \end{bmatrix}$$

$$\rightarrow \tilde{v}_{fly}^{(1,1)} \Big|_{worst-case} = \frac{(M-1)V_{dc}\Delta t L_{cross}}{TL_l}. \tag{51}$$

APPENDIX IV

DERIVATION OF COUPLED INDUCTOR BALANCING CAPABILITIES FOR AN ARBITRARY NUMBER OF LEVELS

We compute the balancing matrix of a two-phase, (K+2)-level converter, which has switching waveforms shown in Fig. 13. First, consider the charge transfers that capacitor #1 of phase #1 induces:

$$Q_{\text{bal}}^{(1,1)\to(1,2)} = (dT)^2 \frac{1}{2L_{\text{corr}}} \tilde{v}_{\text{fly}}^{(1,1)}$$
 (52)

in capacitor #2 of phase #1 and

$$Q_{\text{bal}}^{(1,1)\to(2,1)} = (dT)^2 \frac{1}{L_{\text{cross}}} \tilde{v}_{\text{fly}}^{(1,1)}$$
 (53)

in capacitor #1 of phase #2. A similar pattern exists for the charge transfers of the other flying capacitors, with scaling by the cross inductance for charge induced in the other phase and scaling by the self inductance for charge induced in the other capacitors of the same phase. If we extend this to (K+2)-levels per phase and $d<\frac{1}{2(K+1)}$, the balancing matrix $\mathbf A$ takes the form in eq. (29) with α and β as the element values. $\mathbf A_{(K+2)\text{-levels}}$ is size $2K\times 2K$ since there are two phases with K flying capacitors each. The balancing matrix is skew-symmetric, pentadiagonal, of even size, and Toeplitz, and if $\beta\neq 0$, it has the determinant

$$|\mathbf{A}_{(K+2)\text{-levels}}| = \left[\beta^K U_K(x)\right]^2, \tag{54}$$

where U_K is the Chebyshev polynomial of the second kind of degree K and the argument being the coupling ratio

$$x = \frac{\alpha}{2\beta} = \frac{L_{\text{same}}}{L_{\text{cross}}} = \frac{k}{M - 1 + k} \in (0, 1].$$
 (55)

Eq. (54) indicates that the balancing matrix is singular only at the roots of U_K , which are

$$x_j = \cos\left(\frac{j}{K+1}\pi\right) \tag{56}$$

for $j=1,\ldots,K$. The largest root of U_K is at $x_1=\cos\left(\frac{1}{K+1}\pi\right)$. If the converter coupling ratio x is equal to any of the roots in eq. (56), the converter will not balance. With

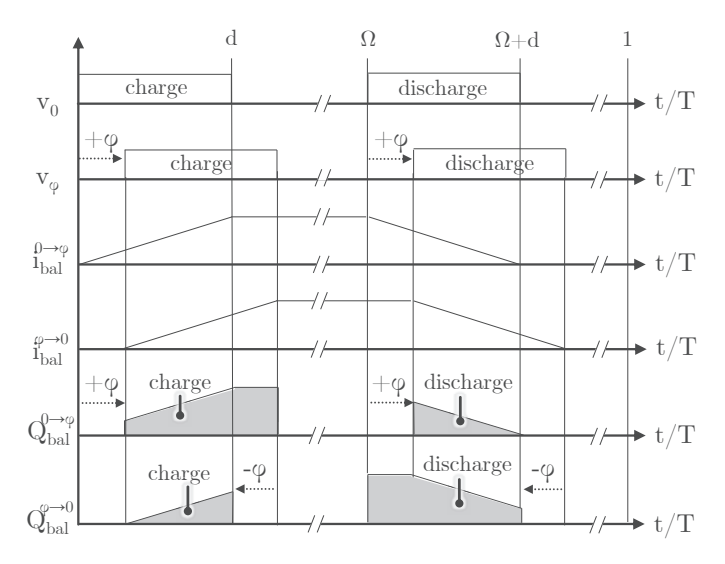


Fig. 31. General charge transfer behavior between two arbitrary phase-shifted flying capacitors in a coupled inductor FCML system.

fully coupled inductors, the coupling ratio $x=\frac{L_{\rm same}}{L_{\rm cross}} \to 1$, which is greater than all of the roots in (56), meaning fully coupled inductors can balance any finite number of levels. For partially coupled inductors with $\frac{L_{\rm same}}{L_{\rm cross}} < 1$, a sufficient condition on the coupling ratio to avoid coinciding with all roots is

$$x = \frac{L_{\text{same}}}{L_{\text{cross}}} > x_1 = \cos\left(\frac{1}{K+1}\pi\right). \tag{57}$$

As the number of levels increases, the largest root x_1 and required coupling ratio increase.

APPENDIX V SINGULARITIES OF THE BALANCING MATRIX

Previously, we only considered specific operating conditions and level/phase combinations to explain coupled inductor balancing. However, the balancing matrix of an M-phase and (K+2)-level FCML converter can have arbitrarily large order and any duty cycle and coupling ratio. In this section, we generalize balancing behavior for any operating conditions from the structure of the balancing matrix.

A. Toeplitz and Skew-Symmetric Properties of the Balancing Matrix

Assuming that the phase shifts between all switches are uniform, the balancing matrix is always Toeplitz and skew-symmetric. To prove this, we consider without loss of generality a flying capacitor called v_0 being connected to the switch node (labelled in Fig. 31), assuming its phase to be zero. This flying capacitor could be from any switching level of a (K+2)-level converter. Every flying capacitor is connected with equal duration in the both a positive and negative orientations in order to maintain charge balancing. In Fig. 31, the phase shift between the flying capacitor being connected again is Ω .

Now we analyze the charge transfer that the flying capacitor induces in another flying capacitor that has its switching actions phase shifted by φ which we call v_{φ} , and the charge

that v_{φ} induces in v_0 . Fig. 31 shows the small-signal imbalance currents and charges induced by each of the flying capacitors in the other. By inspection, we can see that the two flying capacitors are charged and discharged with the same magnitude and opposite signs. Therefore, we can conclude that if a first flying capacitor v_0 induces a charge Q in a flying capacitor v_{φ} , then flying capacitor v_{φ} induces a charge of -Q in v_0 . This is equivalent to saying the balancing matrix must be skew symmetric, since all symmetric entries about the diagonal will have equal magnitude and inverted sign. This proof is uniform across the full operation range and does not depend on the phase shift between the charging and discharging pulses (Ω) , the phase shift between the two capacitors (φ) , or the duty cycle regime.

We now prove that the balancing matrix is Toeplitz. If a flying capacitor, say our base capacitor v_0 , causes a charge transfer Q in another that is phase shifted by φ , then all the flying capacitors will cause the same charge transfer Q in the flying capacitor phase shifted by φ from them. This is a consequence of the symmetry of the converter and the fact that the switching actions are all uniform with equal phase shift. The entries on the same balancing matrix diagonals correspond to equal phase shifts between the flying capacitors, so we can conclude that the balancing matrix must be Toeplitz.

B. Polynomial Determinant of the Balancing Matrix

Generally, each element of the balancing matrix is a polynomial of d scaled by either the $L_{\rm cross}$ or $L_{\rm same}$ inductance. We consider d as a variable and the inductances as fixed since a converter generally has a fixed coupled inductor but can operate across the entire duty cycle regime. Given the varying elements and arbitrary size of $MK \times MK$, it is difficult to explicitly prove the invertibility, and therefore the balancing capability, of the balancing matrix in all cases. However, we can use the skew-symmetric property of the balancing matrix to place bounds on the balancing capability.

First, the determinant of a skew-symmetric matrix of even order can be expressed as a square of a polynomial of its elements [47]. Since the elements are themselves polynomials of d, we know that the determinant of the balancing matrix is a square of a polynomial in d

$$|\mathbf{A}| = (p(d))^2, \tag{58}$$

where p is a polynomial. The degree of the elements of \mathbf{A} can be as large as 2 in d, since the charge transfer elements are calculated as an "area" where the sides are both dependent on the duty cycle. Therefore, as MK is the size of \mathbf{A} , the degree of the polynomial $|\mathbf{A}|$ can be as large as 2MK in d, and the degree of p(d) can be as large as MK in d.

At the roots of p(d), the balancing matrix is singular and balancing fails. Since p(d) is a univariate polynomial of d with degree MK, there are at most MK roots which are generally discrete complex values of d.

C. Limiting Singularities of the Balancing Matrix

The dependence of the balancing matrix on duty cycle changes abruptly at the "nominal" conversion ratios defined

in [31] that are multiples of $\frac{1}{M(K+1)}$. There are generally M(K+1) unique operating regions of the duty cycle bounded by these nominal conversion ratios. The behavior of different regions generally changes when crossing these boundaries because the number of overlapping on-switches changes. The reason there are M(K+1) regions is because there are a total of M(K+1) total switching actions during a switching period, so one phase can overlap between 0 and (M(K+1)-1) other actions, for a total of M(K+1) possibilities.

To explain the different balancing behavior in each duty cycle region, we define i as an index representing the duty cycle operating region of an M-phase, (K+2)-level converter, where the duty cycle in operating region i is in the range $\frac{i-1}{M(K+1)} < d \leq \frac{i}{M(K+1)}$ (bounded by the two nearest nominal conversion ratios). Since there are M(K+1) unique regions, the index can take the values $i=1,2,\ldots M(K+1)$. Formally, the definition of i is

$$i = \operatorname{ceil}(M(K+1)d). \tag{59}$$

We now rewrite the charge balancing equation (18) with explicit reference to the operating region i as

$$\mathbf{Q}_{\text{bal}} + \mathbf{Q}_{\text{dist}} = \mathbf{A}_i(d)\tilde{\mathbf{v}}_{\text{flv}} + \mathbf{Q}_{\text{dist}} = \mathbf{Q}_{\text{cap}}.$$
 (60)

As with before, we assume there is a generic disturbance charge \mathbf{Q}_{dist} injected on the flying capacitors and a balancing charge \mathbf{Q}_{bal} that counters it. The balancing matrix is now written as $\mathbf{A}_i(d)$, where i is the operating region and the dependence on the duty cycle d is highlighted. Finally, the sum of the balancing and disturbance charges is not automatically assumed to be zero, but rather an explicit excess capacitor charge \mathbf{Q}_{cap} . This highlights the fact that if $\mathbf{A}_i(d)$ is singular for a given duty cycle, then it will not be possible to cancel out an arbitrary disturbance.

We can now formally define the duty cycles, if any exist, when balancing fails. Coupled inductor balancing fails for the set of duty cycles

$$\mathcal{D} = \{ d \in (0,1) \, || \mathbf{A}_i(d) | = 0 \} \,. \tag{61}$$

We only consider purely real values of d strictly between 0 and 1 since these are the only non-trivial switching regions. \mathbb{D} specifies all duty cycles in this range which cause the determinant of the corresponding balancing matrix to be zero, which indicates a failure of balancing capability.

There are at most MK roots of $|\mathbf{A}_i(d)| = 0$ for each i. If a root falls within the range $\frac{i-1}{M(K+1)} < d \le \frac{i}{M(K+1)}$, then that root is in \mathcal{D} . If the root falls outside this region or is complex, it is not a practically achievable duty cycle and is not a singularity. Since there are at most MK roots per region i that could be in \mathcal{D} , and M(K+1) total regions, the maximum number of singularities is

$$n(\mathcal{D}) \le M^2 K(K+1),\tag{62}$$

where $n(\mathcal{D})$ is the number of elements in \mathcal{D} . Meanwhile, the maximum number of singularities within a particular duty cycle region defined by i is $n_i < MK$.

These results imply that for a finite number of levels and phases, there is a finite maximum number of duty cycle singularities that can exist, meaning that balancing will generally

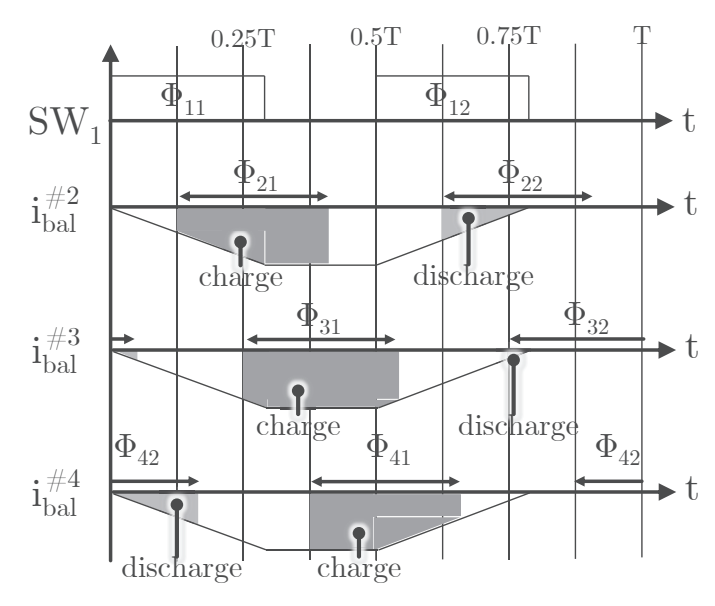


Fig. 32. Balancing currents induced by phase #1 in a four-phase, three-level FCML converter with coupled inductors when the duty cycle is in the range $\frac{1}{4} < d < \frac{3}{8}$.

be possible across the entire duty cycle regime except at specific singular points. We can also conclude that as the number of phases and levels increases, the maximum number of singularities within each duty cycle region i increases while the size of each duty cycle region decreases. Since there are more possible singularities in a smaller space as M and K increase, it is possible that balancing fails for all duty cycles as the number of phases $M \to +\infty$ and/or levels $(K+2) \to +\infty$.

D. Computation of Singularities for Four-Phase Converter

We compute the singularities of a four-phase, three-level FCML converter with $\frac{1}{4} < d \leq \frac{3}{8}$. The balancing matrix in the i=3 operating region may be computed as

$$\mathbf{A}_{i=3}(d) = \frac{T^2}{L_{\text{cross}}} \begin{bmatrix} 0 & \alpha & \beta & \alpha \\ -\alpha & 0 & \alpha & \beta \\ -\beta & -\alpha & 0 & \alpha \\ -\alpha & -\beta & -\alpha & 0 \end{bmatrix}, \tag{63}$$

where

$$\alpha = \frac{d}{8} + \frac{1}{8} \left(d - \frac{1}{8} \right),\tag{64}$$

$$\beta = d^2 - 2\left(d - \frac{1}{4}\right)^2. \tag{65}$$

After computing the determinant and numerically finding the roots of the resulting polynomial of d, we find the set of singular duty cycles for the four-level converter is

$$\mathcal{D} = \{0.2836, 0.3629\}. \tag{66}$$

Coupled inductor cannot help with balancing the flying capacitor voltages at these two singular duty cycles.

REFERENCES

- [1] D. H. Zhou, A. Bendory, P. Wang, and M. Chen, "Intrinsic and robust voltage balancing of fcml converters with coupled inductors," in 2021 IEEE 22nd Workshop on Control and Modelling of Power Electronics (COMPEL), 2021, pp. 1–8.
- [2] D. H. Zhou, A. Bendory, C. Li, and M. Chen, "Multiphase fcml converter with coupled inductors for ripple reduction and intrinsic flying capacitor voltage balancing," in 2022 IEEE Applied Power Electronics Conference and Exposition (APEC), 2022, pp. 1284–1290.
- [3] D. H. Zhou, J. Celikovic, Y. Elasser, D. Maksimovic, and M. Chen, "Balancing limits of flying capacitor voltages in coupled inductor fcml converters," in 2022 IEEE 23rd Workshop on Control and Modeling for Power Electronics (COMPEL), 2022, pp. 1–8.
- [4] X. Zhou, P.-L. Wong, P. Xu, F. Lee, and A. Huang, "Investigation of candidate vrm topologies for future microprocessors," *IEEE Transactions on Power Electronics*, vol. 15, no. 6, pp. 1172–1182, 2000.
- [5] J. Baek, Y. Elasser, K. Radhakrishnan, H. Gan, J. P. Douglas, H. K. Krishnamurthy, X. Li, S. Jiang, C. R. Sullivan, and M. Chen, "Vertical stacked lego-pol cpu voltage regulator," *IEEE Transactions on Power Electronics*, vol. 37, no. 6, pp. 6305–6322, 2022.
- [6] J. Böhler, J. Huber, J. Wurz, M. Stransky, N. Uvaidov, S. Srdic, and J. W. Kolar, "Ultra-high-bandwidth power amplifiers: A technology overview and future prospects," *IEEE Access*, vol. 10, pp. 54613–54633, 2022.
- [7] O. García, M. Vasić, P. Alou, J. Oliver, and J. A. Cobos, "An overview of fast dc–dc converters for envelope amplifier in rf transmitters," *IEEE Transactions on Power Electronics*, vol. 28, no. 10, pp. 4712–4722, 2013.
- [8] T. Meynard and H. Foch, "Multi-level conversion: high voltage choppers and voltage-source inverters," in PESC '92 Record. 23rd Annual IEEE Power Electronics Specialists Conference, 1992, pp. 397–403 vol.1.
- [9] R. H. Wilkinson, T. A. Meynard, and H. du Toit Mouton, "Natural balance of multicell converters: The two-cell case," *IEEE Transactions* on *Power Electronics*, vol. 21, no. 6, pp. 1649–1657, 2006.
- [10] R. H. Wilkinson, T. A. Meynard, and H. du Toit Mouton, "Natural balance of multicell converters: The general case," *IEEE Transactions* on *Power Electronics*, vol. 21, no. 6, pp. 1658–1666, 2006.
- [11] R. Wilkinson, H. du Mouton, and T. Meynard, "Natural balance of multicell converters," in *IEEE 34th Annual Conference on Power Electronics Specialist*, 2003. PESC '03., vol. 3, 2003, pp. 1307–1312 vol.3.
- [12] B. P. McGrath and D. G. Holmes, "Analytical modelling of voltage balance dynamics for a flying capacitor multilevel converter," in 2007 IEEE Power Electronics Specialists Conference, 2007, pp. 1810–1816.
- [13] ——, "Enhanced voltage balancing of a flying capacitor multilevel converter using phase disposition (pd) modulation," *IEEE Transactions* on *Power Electronics*, vol. 26, no. 7, pp. 1933–1942, 2011.
- [14] V. Lazarević, "Ultra-fast and compact gan-based power amplifier as an arbitrary voltage generator," Ph.D. dissertation, Universidad Politécnica de Madrid, 2021.
- [15] P. S. Niklaus, J. W. Kolar, and D. Bortis, "100 khz large-signal bandwidth gan-based 10 kva class-d power amplifier with 4.8 mhz switching frequency," *IEEE Transactions on Power Electronics*, vol. 38, no. 2, pp. 2307–2326, 2023.
- [16] C. B. Barth, P. Assem, T. Foulkes, W. H. Chung, T. Modeer, Y. Lei, and R. C. N. Pilawa-Podgurski, "Design and control of a gan-based, 13level, flying capacitor multilevel inverter," *IEEE Journal of Emerging* and Selected Topics in Power Electronics, vol. 8, no. 3, pp. 2179–2191, 2020.
- [17] T. Modeer, C. B. Barth, N. Pallo, W. H. Chung, T. Foulkes, and R. C. N. Pilawa-Podgurski, "Design of a gan-based, 9-level flying capacitor multilevel inverter with low inductance layout," in 2017 IEEE Applied Power Electronics Conference and Exposition (APEC), 2017, pp. 2582–2589.
- [18] C. Suthar, V. I. Kumar, F. Alskran, and D. Maksimović, "An arbitrary waveform generator based on an eight-level flying-capacitor multilevel converter," in 2021 IEEE Applied Power Electronics Conference and Exposition (APEC), 2021, pp. 1008–1014.
- [19] S. Coday, A. Barchowsky, and R. C. Pilawa-Podgurski, "A 10-level gan-based flying capacitor multilevel boost converter for radiationhardened operation in space applications," in 2021 IEEE Applied Power Electronics Conference and Exposition (APEC), 2021, pp. 2798–2803.
- [20] J. Li, C. Sullivan, and A. Schultz, "Coupled-inductor design optimization for fast-response low-voltage dc-dc converters," in APEC. Seventeenth Annual IEEE Applied Power Electronics Conference and Exposition (Cat. No.02CH37335), vol. 2, 2002, pp. 817–823 vol.2.

- [21] K. J. Hartnett, J. G. Hayes, M. G. Egan, and M. S. Rylko, "Cctt-core split-winding integrated magnetic for high-power dc-dc converters," *IEEE Transactions on Power Electronics*, vol. 28, no. 11, pp. 4970–4984, 2013.
- [22] P.-L. Wong, P. Xu, P. Yang, and F. Lee, "Performance improvements of interleaving vrms with coupling inductors," *IEEE Transactions on Power Electronics*, vol. 16, no. 4, pp. 499–507, 2001.
- [23] D. H. Zhou, Y. Elasser, J. Baek, and M. Chen, "Reluctance-based dynamic models for multiphase coupled inductor buck converters," *IEEE Transactions on Power Electronics*, vol. 37, no. 2, pp. 1334–1351, 2022.
- [24] M. Chen and C. R. Sullivan, "Unified models for coupled inductors applied to multiphase pwm converters," *IEEE Transactions on Power Electronics*, vol. 36, no. 12, pp. 14155–14174, 2021.
- [25] P. Wang, D. H. Zhou, Y. Elasser, J. Baek, and M. Chen, "Matrix coupled all-in-one magnetics for pwm power conversion," *IEEE Transactions on Power Electronics*, vol. 37, no. 12, pp. 15035–15050, 2022.
- [26] T. Meynard, M. Fadel, and N. Aouda, "Modeling of multilevel converters," *IEEE Transactions on Industrial Electronics*, vol. 44, no. 3, pp. 356–364, 1997.
- [27] S. Thielemans, A. Ruderman, B. Reznikov, and J. Melkebeek, "Improved natural balancing with modified phase-shifted pwm for single-leg fivelevel flying-capacitor converters," *IEEE Transactions on Power Electronics*, vol. 27, no. 4, pp. 1658–1667, 2012.
- [28] J. S. Rentmeister and J. T. Stauth, "Modeling the dynamic behavior of hybrid-switched-capacitor converters in state space," in 2018 IEEE 19th Workshop on Control and Modeling for Power Electronics (COMPEL), 2018, pp. 1–7.
- [29] N. C. Brooks, R. K. Iyer, R. S. Bayliss, and R. C. N. Pilawa-Podgurski, "Fundamental state-space modeling methodology for the flying capacitor multilevel converter," in 2022 IEEE 23rd Workshop on Control and Modeling for Power Electronics (COMPEL), 2022, pp. 1–7.
- [30] L. Corradini and D. Maksimović, "Steady-state indeterminacy in lossless switched-mode power converters," *IEEE Transactions on Power Elec*tronics, vol. 38, no. 3, pp. 3001–3013, 2023.
- [31] Z. Xia, B. L. Dobbins, and J. T. Stauth, "Natural balancing of flying capacitor multilevel converters at nominal conversion ratios," in 2019 20th Workshop on Control and Modeling for Power Electronics (COMPEL), 2019, pp. 1–8.
- [32] Z. Xia, B. L. Dobbins, J. S. Rentmeister, and J. T. Stauth, "State space analysis of flying capacitor multilevel dc-dc converters for capacitor voltage estimation," in 2019 IEEE Applied Power Electronics Conference and Exposition (APEC), 2019, pp. 50–57.
- [33] J. Celikovic, R. Das, H.-P. Le, and D. Maksimovic, "Modeling of capacitor voltage imbalance in flying capacitor multilevel dc-dc converters," in 2019 20th Workshop on Control and Modeling for Power Electronics (COMPEL), 2019, pp. 1–8.
- [34] J. S. Rentmeister and J. T. Stauth, "A 48v:2v flying capacitor multilevel converter using current-limit control for flying capacitor balance," in 2017 IEEE Applied Power Electronics Conference and Exposition (APEC), 2017, pp. 367–372.
- [35] A. Stillwell, E. Candan, and R. C. N. Pilawa-Podgurski, "Active voltage balancing in flying capacitor multi-level converters with valley current detection and constant effective duty cycle control," *IEEE Transactions* on *Power Electronics*, vol. 34, no. 11, pp. 11429–11441, 2019.
- [36] S. d. Silva Carvalho, N. Vukadinović, and A. Prodić, "Phase-shift control of flying capacitor voltages in multilevel converters," in 2020 IEEE Applied Power Electronics Conference and Exposition (APEC), 2020, pp. 299–304.
- [37] Z. Xia and J. T. Stauth, "Constant switch stress control of hybrid switched capacitor dc-dc converters," in 2022 IEEE Applied Power Electronics Conference and Exposition (APEC), 2022, pp. 1214–1221.
- [38] A. Ruderman and B. Reznikov, "Five-level single-leg flying capacitor converter voltage balance dynamics analysis," in 2009 35th Annual Conference of IEEE Industrial Electronics, 2009, pp. 486–491.
- [39] S. Thielemans, A. Ruderman, and J. Melkebeek, "Flying-capacitor multilevel converter voltage balance dynamics for pure resistive load," in 2009 8th International Symposium on Advanced Electromechanical Motion Systems Electric Drives Joint Symposium, 2009, pp. 1–6.
- [40] Z. Ye, Y. Lei, Z. Liao, and R. C. N. Pilawa-Podgurski, "Investigation of capacitor voltage balancing in practical implementations of flying capacitor multilevel converters," *IEEE Transactions on Power Electronics*, vol. 37, no. 3, pp. 2921–2935, 2022.
- [41] R. Das, J. Celikovic, S. Abedinpour, M. Mercer, D. Maksimovic, and H.-P. Le, "Demystifying capacitor voltages and inductor currents in hybrid converters," in 2019 20th Workshop on Control and Modeling for Power Electronics (COMPEL), 2019, pp. 1–8.

- [42] D. Floricau, G. Gateau, and T. A. Meynard, "New multilevel flying-capacitor inverters with coupled-inductors," in 2012 13th International Conference on Optimization of Electrical and Electronic Equipment (OPTIM), 2012, pp. 764–769.
- [43] P.-L. Wong, "Performance improvements of multi-channel interleaving voltage regulator modules with integrated coupling inductors," Ph.D. dissertation, Virginia Tech., 2001.
- [44] J. Azurza Anderson, G. Zulauf, P. Papamanolis, S. Hobi, S. Mirić, and J. W. Kolar, "Three levels are not enough: Scaling laws for multilevel converters in ac/dc applications," *IEEE Transactions on Power Electronics*, vol. 36, no. 4, pp. 3967–3986, 2021.
- [45] J. Rodriguez, L. G. Franquelo, S. Kouro, J. I. Leon, R. C. Portillo, M. M. Prats, and M. A. Perez, "Multilevel converters: An enabling technology for high-power applications," *Proceedings of the IEEE*, vol. 97, no. 11, pp. 1786–1817, 2009.
- [46] Y. Elasser, J. Baek, C. R. Sullivan, and M. Chen, "Modeling and design of vertical multiphase coupled inductors with inductance dual model," in 2021 IEEE Applied Power Electronics Conference and Exposition (APEC), 2021, pp. 1717–1724.
- [47] W. Ledermann, "A note on skew-symmetric determinants," Proceedings of the Edinburgh Mathematical Society, vol. 36, no. 2, pp. 335–338, 1993



Dragan Maksimović (M'89—SM'04—F'15) received the B.S. and M.S. degrees in electrical engineering from the University of Belgrade, Serbia, in 1984 and 1986, respectively, and the Ph.D. degree from the California Institute of Technology, Pasadena, CA, USA, in 1989. From 1989 to 1992, he was with the University of Belgrade. Since 1992, he has been with the Department of Electrical, Computer and Energy Engineering, University of Colorado, Boulder, CO, USA, where he is currently a Distinguished Professor and Co-Director of the

Colorado Power Electronics Center. He has coauthored more than 300 publications and the textbooks Fundamentals of Power Electronics and Digital Control of High-Frequency Switched-Mode Power Converters. His current research interests include power electronics for renewable energy sources and energy efficiency, high-frequency power conversion using wide-bandgap semiconductors, and digital control of switched-mode power converters.

Prof. Maksimović received the 1997 National Science Foundation CAREER Award, the IEEE Power Electronics Society (IEEE PELS) Transactions Prize Paper Award in 1997, the IEEE PELS Prize Letter Awards in 2009 and 2010, the University of Colorado Inventor of the Year Award in 2006, the IEEE PELS Modeling and Control Technical Achievement Award for 2012, the Holland Excellence in Teaching Awards in 2004, 2011 and 2018, the Charles Hutchinson Memorial Teaching Award for 2012, the 2013 Boulder Faculty Assembly Excellence in Teaching Award, the 2020 College of Engineering and Applied Sciences Research Award, the 2022 IEEE PELS R. David Middlebrook Achievement Award, and the 2023 IEEE William E. Newell Power Electronics Award.



Daniel H. Zhou (Student Member, IEEE) received the B.A.Sc degree in mechatronics engineering from the University of Waterloo, Waterloo, Canada, in 2019. He received the M.A. degree in electrical engineering from Princeton University, Princeton, NJ, USA in 2021 and is currently working towards the Ph.D. degree.

His research interests include ultrafast power converters, multilevel converters, and advanced power magnetics design. Mr. Zhou is a recipient of the IEEE PELS John G. Kassakian Fellowship and the

Natural Sciences and Engineering Research Council of Canada (NSERC) Alexander Graham Bell Graduate Scholarship. He is also an awardee of the Princeton School of Engineering and Applied Science Honorific Fellowship and Graduate Student Award for Excellence in Service.



Minjie Chen (Senior Member, IEEE) received the S.M., E.E., and Ph.D. degrees in electrical engineering and computer science from Massachusetts Institute of Technology, Cambridge, MA, USA, in 2015 and the B.S. degree in electrical engineering from Tsinghua University, Beijing, China, in 2009. He is an Assistant Professor of electrical and computer engineering and the Andlinger Center for Energy and the Environment at Princeton University. His research interests include modeling, design, and application of high-performance power electronics.

Dr. Chen is a recipient of the IEEE PELS Richard M. Bass Outstanding Young Power Electronics Engineer Award, the Princeton SEAS E. Lawrence Keyes, Jr./Emerson Electric Co. Junior Faculty Award, the NSF CAREER Award, six IEEE Transactions on Power Electronics Prize Paper Awards, the MIT EECS D. N. Chorafas Ph.D. Thesis Award, and numerous conference paper awards from COMPEL, ICRA, IROS, ECCE, APEC, 3D-PEIM, and OCP. He was listed on the Princeton Engineering Commendation List for Outstanding Teaching multiple times. He is an IEEE PELS Distinguished Lecturer, the vice chair of IEEE PELS TC10-Design Methodologies, and is the co-founder of the IEEE PELS MagNet Challenge.



Janko Čeliković (Member, IEEE) received the B.S. and M.S. degrees in electrical engineering from the University of Belgrade, Belgrade, Serbia in 2016 and 2018, respectively, and the Ph.D. degree from the Colorado Power Electronics Center (CoPEC), University of Colorado, Boulder, CO, USA, in 2022. From 2020 to 2022, he was a part-time PMIC Design Engineering Intern with Renesas Electronics (formerly Dialog Semiconductor). He is currently a Senior Analog Design Engineer at Renesas Electronics. His research interests include digital control of

switched-mode power converters, PMIC design, and modeling of hybrid and multilevel power converters. Dr. Čeliković was the recipient of Technical Session Best Presentation Award at IEEE APEC 2021, and coauthored the paper that received the Best Paper Award at IEEE COMPEL 2019.